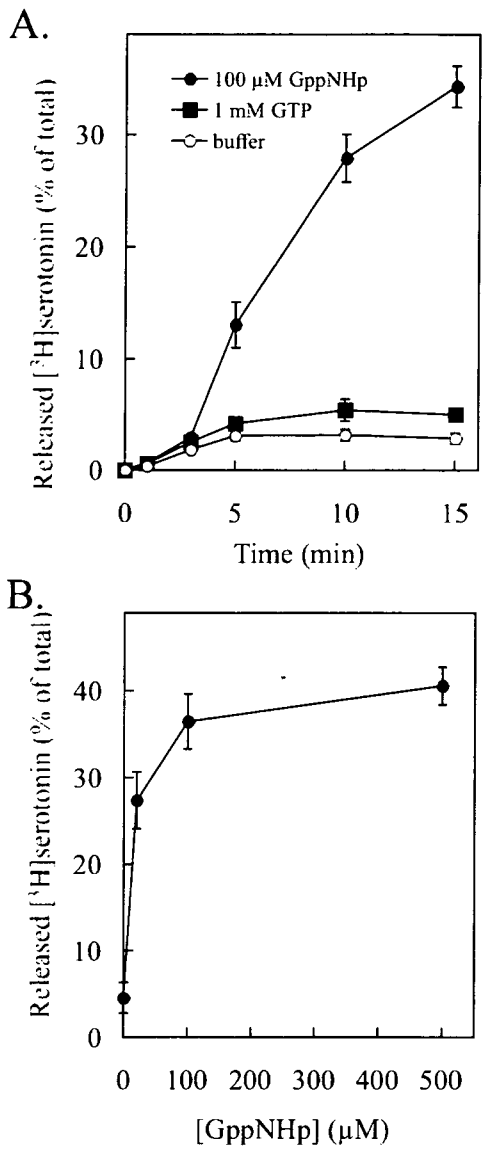

FIGURE 1. **GppNHp-induced dense granule secretion from permeabilized platelets.** Permeabilized platelets were stimulated with buffer alone (*open circles*), 1 mM GTP (*closed squares*), or 100 μM GppNHp (*closed circles*) for the indicated periods at 30 °C (*A*) or with various concentrations of GppNHp for 15 min at 30 °C (*B*). Released [³H]serotonin was measured as described under "Experimental Procedures." Values are means ± S.E. from three independent experiments.

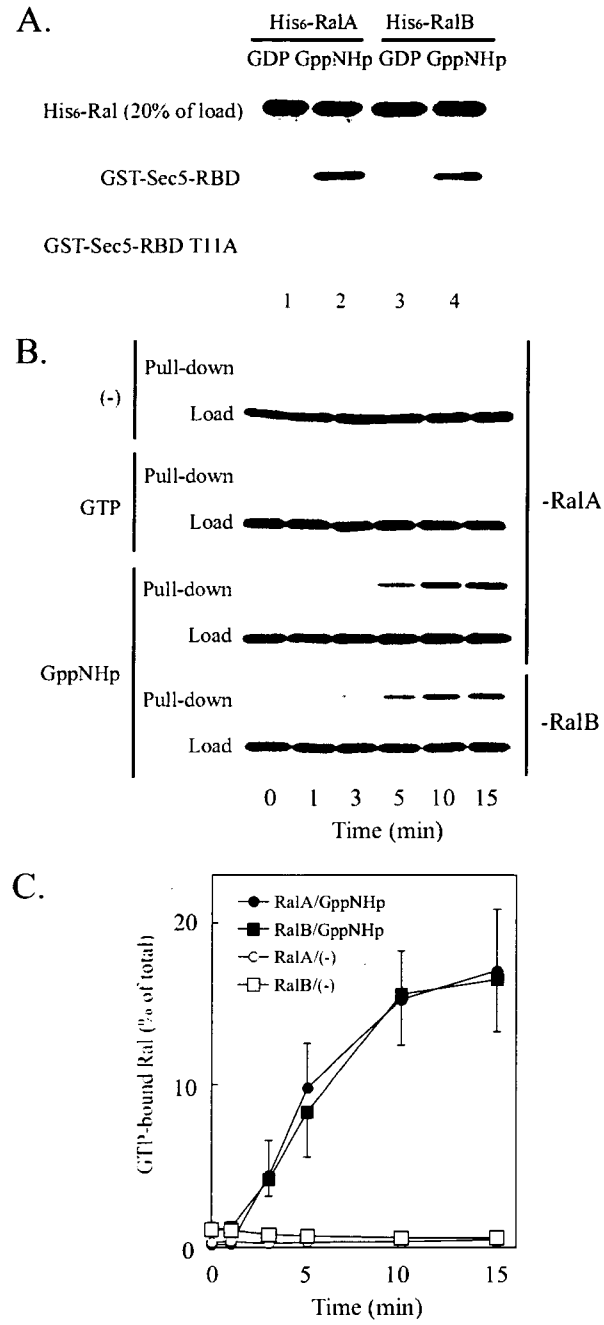

FIGURE 2. **The time-dependent activation of Ral upon stimulation with GppNHp in permeabilized platelets.** *A*, GDP-bound (*lanes 1* and *3*) or GppNHp-bound His_6-RalA and -RalB (*lanes 2* and *4*) were incubated with glutathione-Sepharose beads coated with wild-type GST-Sec5-RBD (*middle panel*) and GST-Sec5-RBD T11A (*lower panel*) at 4 °C for 1 h. After washing the beads, bead-associated His_6-RalA and -RalB were detected by immunoblotting with anti-His_6 antibody as described under "Experimental Procedures". *B* and *C*, permeabilized platelets were stimulated with buffer alone, 1 mM GTP, or 100 μM GppNHp for indicated periods at 30 °C. GTP (GppNHp)-bound RalA and RalB were measured by the GTP-Ral pulldown assay using the GST-Sec5-RBD as described under "Experimental Procedures." The data shown are representative (*B*) and means ± S.E. (*C*) of three independent experiments.

Involvement of the Exocyst Complex in the GppNHp-induced Dense Granule Secretion from Permeabilized Platelets—Among the effector molecules of Ral, exocyst complex could be a candidate for mediating the GppNHp-induced secretion from permeabilized platelets. To examine this possibility, we first confirmed the existence of the exocyst complex in platelet extracts by affinity chromatography. As shown in Fig. 4*A*, seven protein bands ranging in molecular mass from 70 to 110 kDa were specifically detected in the GTPγS-RalA lane (*lane 3*). MALDI-TOF MS analysis of these proteins identified all the eight components of the human exocyst complex and another Ral effector, Ral-binding protein 1 (RalBP1). Human Sec15 protein is composed of two isoforms that share 66% identity and 75% similarity (24); we detected both Sec15-like 1 and -like 2 isoforms in human platelets.

Subcellular distribution analysis revealed that RalA was exclusively membrane-bound, whereas the exocyst complex

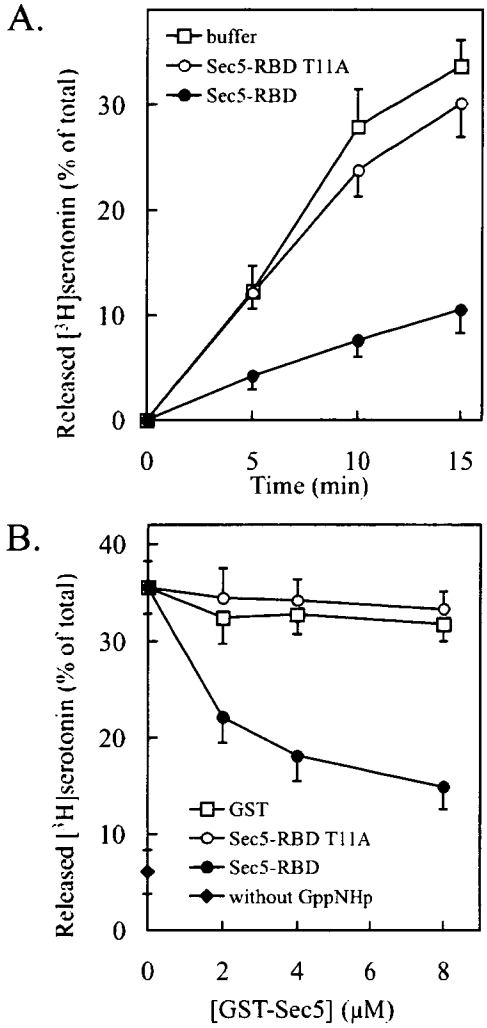

FIGURE 3. **Sec5-RBD inhibited the GppNHp-induced dense granule secretion from permeabilized platelets.** *A*, permeabilized platelets were first incubated with buffer alone (*open squares*), 8 μM GST-Sec5-RBD (*closed circles*), or 8 μM GST-Sec5-RBD T11A (*open circles*) at 4 °C for 15 min and stimulated with 100 μM GppNHp for indicated periods at 30 °C. Released [³H]serotonin was measured as described under "Experimental Procedures." *B*, permeabilized platelets were first incubated with various concentrations of GST (*open squares*), GST-Sec5-RBD (*closed circles*), or GST-Sec5-RBD T11A (*open circles*) at 4 °C for 15 min and stimulated with 100 μM GppNHp at 30 °C for 15 min. Released [³H]serotonin was measured as described under "Experimental Procedures." The secretion without the GppNHp stimulation is also shown (◆). Values are means ± S.E. from three independent experiments.

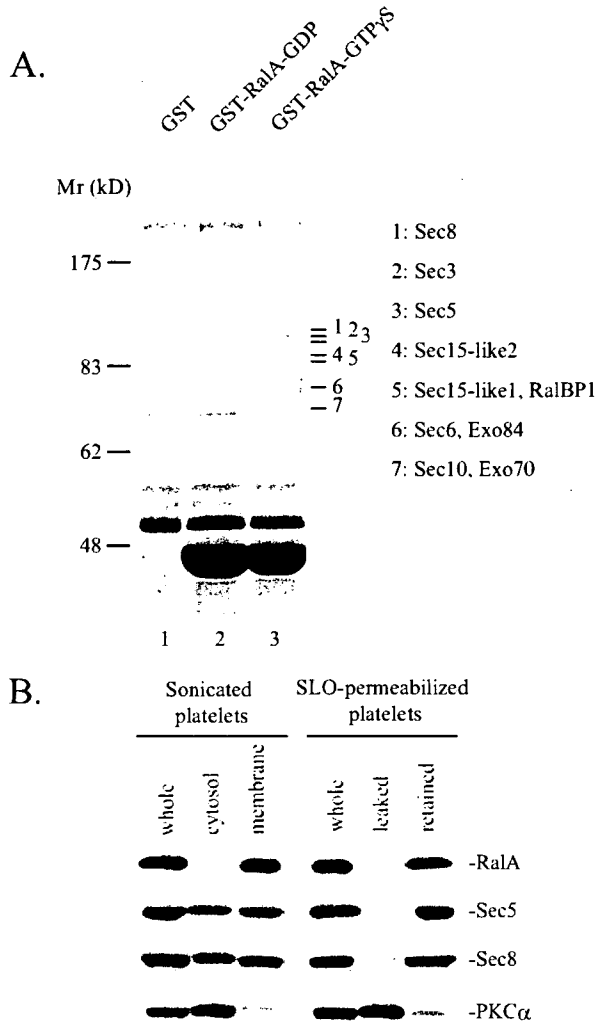

FIGURE 4. **Identification and subcellular distribution of the exocyst complex in platelets.** *A*, glutathione-Sepharose beads coated with GST alone (*lane 1*), GDP-bound (*lane 2*), or GTPγS-bound GST-RalA (*lane 3*) were incubated with platelet cytosol at 4 °C for 1 h. After washing the beads, bead-associated proteins were analyzed by electrophoresis on an SDS-polyacrylamide gel (4–20%) and stained with Coomassie Blue as described under "Experimental Procedures." Seven protein bands ranging in molecular mass from 70 to 110 kDa were specifically detected in *lane 3*. These proteins were analyzed by MALDI-TOF MS, and the results are shown on the *right* of the gel. *B*, isolated platelets were sonicated (*left panel*). After centrifugation, the supernatant was regarded as cytosolic fraction and the pellet as membrane-bound fraction. SLO-permeabilized platelets were incubated at 4 °C for 15 min (*right panel*). After centrifugation, the supernatant was regarded as fraction leaked out from the cells and the pellet as fraction retained in the cells. Comparable amounts of the supernatants and the pellets were analyzed by immunoblotting with anti-RalA, anti-Sec5-N terminus, anti-Sec8, and anti-PKCα antibodies as described under "Experimental Procedures."

was equally distributed in both cytosol and membrane fractions of intact platelets (*left panel* in Fig. 4*B*). In SLO-permeabilized platelets, most of the exocyst complex was retained in the cells, possibly because of its large size, in the condition where most of PKCα, a cytosolic protein, leaked out from the cells by diffusion (*right panel* in Fig. 4*B*). These results might explain why exogenous addition of platelet cytosol was dispensable for the GppNHp-induced secretion from permeabilized platelets but not for the Ca^{2+}-induced secretion (38).

To examine the involvement of the exocyst complex in the secretion, an anti-Sec5-RBD antiserum was raised in rabbits by injecting GST-Sec5-RBD (amino acids 1–120) as an antigen. We first affinity-purified the antibody against the GST part of the fusion protein from the antiserum and then used the anti-GST antibody as a control in the following experiments. Subsequently, anti-Sec5-RBD antibody was affinity-purified from serum depleted of anti-GST antibodies. In Western blot analysis, the anti-Sec5-RBD antibody recognized a single band at 100 kDa in the platelet lysate, which was the expected molecular mass of Sec5 (Fig. 5*A*). This antibody immunoprecipitated not only Sec5 but also Sec8 from human platelet cytosol (Fig. 5*B*), implying that the anti-Sec5-RBD antibody was capable of immunoprecipitating the entire exocyst complex. Further-

more, this antibody, but not the anti-GST antibody, concentration-dependently inhibited the interaction of Sec5 and Sec8 with GppNHp-RalA *in vitro* (Fig. 5*C*), indicating that the anti-Sec5-RBD antibody abrogated the interaction between Ral and the exocyst complex. Importantly, the addition of the anti-Sec5-RBD antibody inhibited the GppNHp-induced dense granule secretion in a concentration-dependent manner (Fig. 5*D*). In contrast, the anti-GST antibody or control rabbit IgG had no effect (Fig. 5*D*). These results indicated that the exocyst complex played an essential role for the GppNHp-induced dense granule secretion through interaction with active Ral.

GppNHp-bound Ral Increased the Ca^{2+} Sensitivity of Dense Granule Secretion in Permeabilized Platelets—An increase in intracellular Ca^{2+} concentration is considered to be the trigger for the platelet secretion (6). To determine whether Ral was involved in the regulation of the Ca^{2+}-induced dense granule secretion, we analyzed the effects of GppNHp and Sec5-RBD on dense granule secretion induced by various concentrations of Ca^{2+} in permeabilized platelets. In the absence of GppNHp, the threshold for activation of [^{3}H]serotonin release by Ca^{2+} was ~600 nM, with maximal release occurring at 2 μM (*closed squares* in Fig. 6). The addition of 100 μM GppNHp shifted the Ca^{2+} concentration-response curve for [^{3}H]serotonin release to the left (*closed circles* in Fig. 6) as shown previously (7) and resulted in a decrease in the Ca^{2+} concentration required for half-maximal secretion from 1.2 μM to 90 nM. These data indicated that 100 μM GppNHp increased the Ca^{2+} sensitivity of dense granule secretion by ~13-fold. Importantly, this increase in the Ca^{2+} sensitivity of the secretion was inhibited by the addition of Sec5-RBD (*open circles* in Fig. 6), indicating the involvement of GTP-Ral in increasing the Ca^{2+} sensitivity of dense granule secretion from permeabilized platelets. The effect of Sec5-RBD was specific because the addition of Sec5-RBD alone had no effect on Ca^{2+}-induced dense granule secretion (*open squares* in Fig. 6).

Thrombin Induced the Association of Ral with the Exocyst Complex in Intact Platelets—In the last set of experiments, we examined whether the Ral and the exocyst complex could function in intact platelets. Thrombin is a potent agonist for platelets. Thrombin rapidly induced the release of serotonin stored in dense granules in intact platelets (Fig. 7*A*). Moreover, thrombin immediately activated both RalA and RalB in a similar time course to that of the secretion (Fig. 7, *B* and *C*). Both RalA and RalB were maximally activated at 30 s after thrombin stimulation, and the ratio of activated RalA or RalB to total was ~ 6% (Fig. 7*C*). To examine the possible involvement of the Ral-exocyst pathway in intact platelets, we analyzed the association between Ral and the exocyst complex upon thrombin stimulation. As shown in Fig. 7*D*, anti-Sec8 antibody precipitated little RalA before thrombin stimulation, whereas RalA was clearly detected in the immunoprecipitates with anti-Sec8 antibody after 60 s of stimulation. Thus, thrombin induced the association of Ral with the exocyst complex in a similar time course to that of the secretion (Fig. 7*A*) and Ral activation (Fig. 7, *B* and *C*), suggesting that the Ral-exocyst pathway could function in intact platelets.

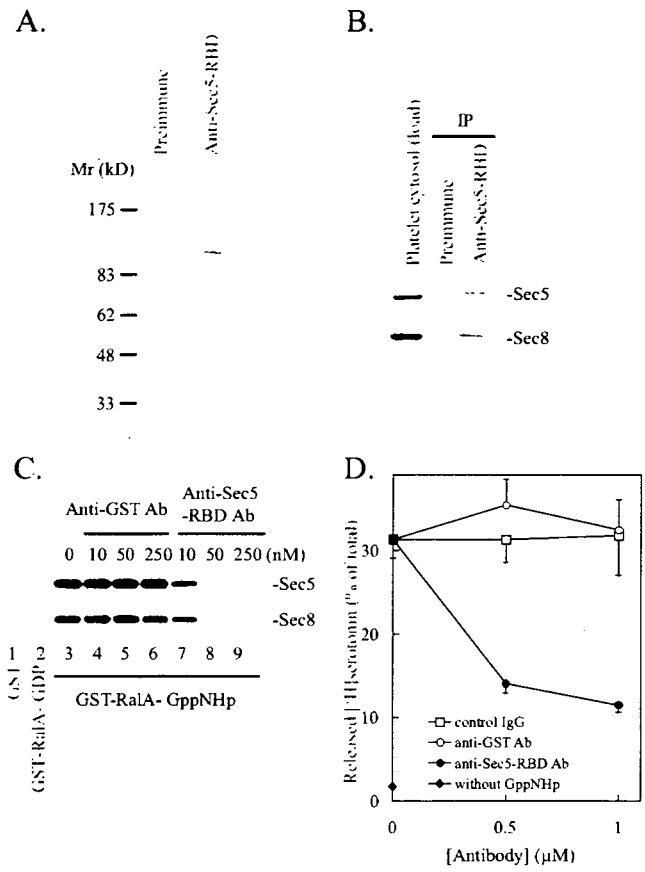

FIGURE 5. **Anti-Sec5-RBD antibody blocked binding of Ral to the exocyst complex and inhibited the GppNHp-induced dense granule secretion.** *A*, human platelet lysates (30 μg of proteins) were immunoblotted with preimmune serum and anti-Sec5-RBD antibody. *B*, human platelet cytosol was immunoprecipitated (*IP*) with preimmune serum and anti-Sec5-RBD antibody. Immunoprecipitated proteins were detected with anti-Sec5-RBD antibody and anti-Sec8 monoclonal antibody. *C*, glutathione-Sepharose beads coated with GST alone (*lane 1*), GDP-bound (*lane 2*), or GppNHp-bound GST-RalA (*lanes 3–9*) were incubated with the platelet cytosols in the presence of anti-GST antibody (*Ab*) (*lane 4–6*) or anti-Sec5-RBD antibody (*lane 7–9*) at 4 °C for 1 h. After washing the beads, bead-associated proteins were analyzed by immunoblotting with anti-Sec5-N-teminus polyclonal antibody and anti-Sec8 monoclonal antibody. The data shown are representative of three independent experiments with similar results. *D*, permeabilized platelets were first incubated with various concentrations of rabbit IgG (*open squares*), anti-GST antibody (*open circles*) and anti-Sec5-RBD antibody (*closed circles*) at 4 °C for 30 min and stimulated with 100 μM GppNHp at 30 °C for 15 min. Released [^{3}H]serotonin was measured as described under "Experimental Procedures." The secretion without the GppNHp stimulation is also shown (◆). Values are means ± S.E. from three independent experiments.

DISCUSSION

It has long been known that non-hydrolyzable GTP analogues induce granule secretion from permeabilized platelets (7–11). Here we demonstrated that Ral GTPase and the exocyst complex mediated this GppNHp-induced dense granule secretion. We also showed that GTP-Ral enhanced the Ca^{2+} sensitivity of dense granule secretion from permeabilized platelets, and the Ral-exocyst pathway could play a role in intact platelets.

In this study, we demonstrated the involvement of Ral by showing that Sec5-RBD, which is a specific inhibitor of Ral, affected the secretion. The effect is specific because the Sec5-RBD T11A mutant that lacks the GTP-Ral binding activity (35) did not inhibit the secretion (Fig. 3, *A* and *B*). The time course of

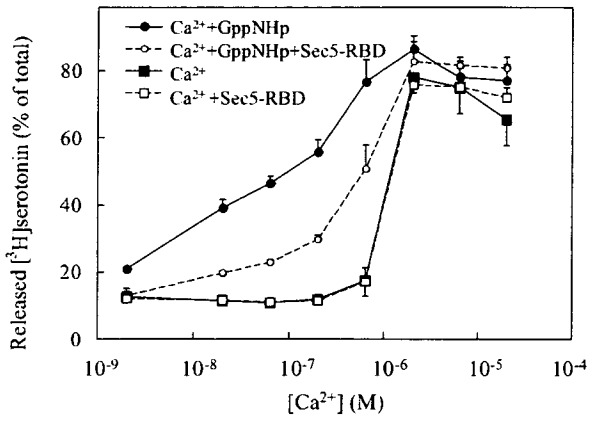

FIGURE 6. **The effects of GppNHp on dense granule secretion induced by various concentrations of Ca^{2+} in permeabilized platelets.** Permeabilized platelets were incubated with various concentrations of Ca^{2+} (*closed squares*) with addition of 8 μM GST-Sec5-RBD (*open squares*), 100 μM GppNHp (*closed circles*), or 100 μM GppNHp and 8 μM GST-Sec5-RBD (*open circles*) at 4 °C for 15 min in the presence of human platelet cytosols (1.0 mg of protein/ml). Samples were then stimulated at 30 °C for 10 min, and released [^{3}H]serotonin was measured as described under "Experimental Procedures." Values are means ± S.E. from three independent experiments.

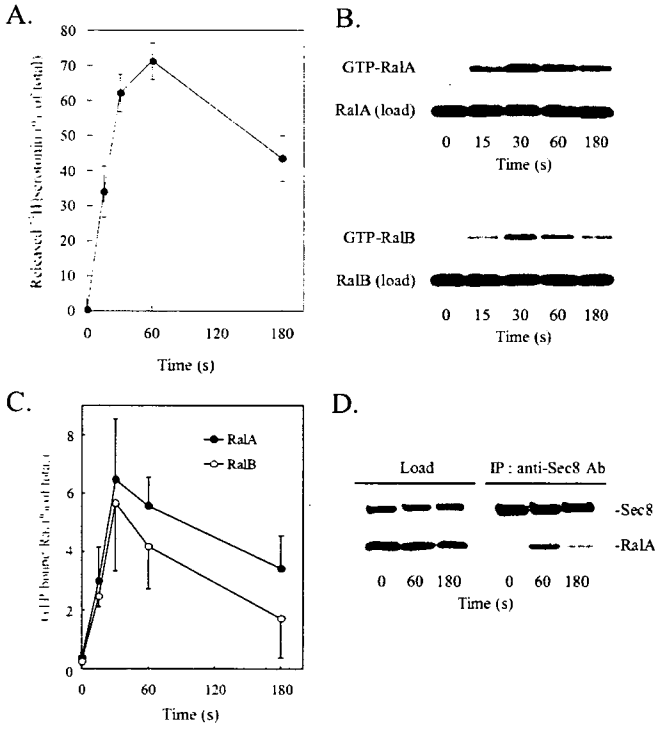

FIGURE 7. **Thrombin induced the rapid activation of Ral and the interaction of Ral with the exocyst complex in intact platelets.** *A–C*, isolated platelets were stimulated with 0.5 unit/ml thrombin for indicated periods at 30 °C. Released [^{3}H]serotonin (*A*) and GTP-bound RalA and RalB (*B* and *C*) were measured as described under "Experimental Procedures." The data shown are expressed as means ± S.E. (*A* and *C*) and are representative of three independent experiments (*B*). *D*, isolated platelets were stimulated with 0.5 unit/ml thrombin for indicated periods at 30 °C. The lysates of the platelets were incubated with anti-Sec8 polyclonal antibody-loaded protein A-agarose beads at 4 °C for 1 h. Immunoprecipitated proteins were detected with anti-RalA antibody as described under "Experimental Procedures." The data shown are representative of three independent experiments with similar results.

the GppNHp-induced secretion from permeabilized platelets is more than 10 times slower than that of the thrombin-induced secretion from intact platelets (compare Figs. 1*A* and 7*A*). This could be because of slow conversion of GDP to GppNHp on Ral in permeabilized platelets (Fig. 2, *B* and *C*). Furthermore, incubation of permeabilized platelets with GTP did not activate Ral (Fig. 2*B*) and did not induce appreciable secretion (Fig. 1*A*). This could be because of the strong GTPase-activating protein activity for Ral in permeabilized platelets. We consider that the decrease of GTP-Ral after the transient activation in thrombin-stimulated intact platelets is due to GTPase-activating protein activity in the cells, where GTP bound to Ral would be rapidly hydrolyzed to GDP (Fig. 7, *B* and *C*). On the other hand, in permeabilized platelets incubated with GppNHp, GppNHp would not be hydrolyzed once bound to Ral (Fig. 2). Therefore, we could observe the apparent difference in the time courses of the ratio of GTP-Ral between thrombin-stimulated intact platelets and GppNHp-incubated permeabilized platelets. GTPase-activating protein activity for Ral could also explain the reason why the maximal ratio of activated Ral to total in intact platelets (~6%) was lower than that in permeabilized platelets (~17%) (compare Figs. 7*C* and 2*C*).

To distinguish the role of RalA from that of RalB, we must, for example, knock down RalA or RalB in platelets or use platelets of either RalA or RalB knock-out mice. However, they are not technically available at the moment. Therefore, we could not distinguish their effects because Sec5-RBD, used as a Ral inhibitor, interacted with both RalA and RalB to a similar extent *in vitro* (Fig. 2*A*). Both RalA and RalB are present in platelets, highly similar (sharing 85% identity) (18, 19), and equally activated by agonist stimulation in intact platelets (Fig. 7, *B* and *C*). Hence, both RalA and RalB might play roles in the secretion in platelets.

Ral has several effectors (18, 19). Among them, the exocyst complex has been implicated in exocytosis. Wang *et al.* (46) showed that Sec5-RBD inhibits the GppNHp-induced granule secretion from permeabilized neuroendocrine PC12 cells, indicating that this secretion is Ral-dependent. They further showed that unprenylated wild-type RalA inhibits the GppNHp-induced secretion, but RalA E38R mutant lacking the Sec5 binding activity has no effect. They concluded that the exocyst complex is involved in the secretion (46). Strictly, however, if we assume a putative Ral effector that does not bind to RalA E38R, it is difficult to exclude the possibility that Ral mediates the secretion through such an effector but not the exocyst complex. Therefore, to demonstrate the involvement of the exocyst complex, we need, for example, to examine the effect of knockdown of an exocyst component or an inhibitory antibody against an exocyst component on the secretion. Here, we demonstrated the involvement of the exocyst complex by showing that an antibody against Sec5-RBD inhibited the GppNHp-induced secretion from permeabilized platelets (Fig. 5*D*).

In addition to Sec5, Exo84, another component of the exocyst complex, also binds to active Ral (27, 28). However, the anti-Sec5-RBD antibody used here completely abolished the interaction between Ral and the exocyst complex *in vitro* (Fig. 5*C*), suggesting that the Ral-Sec5 interaction is dominant com-

pared with the Ral-Exo84 interaction, although we cannot exclude the possibility that the steric hindrance by the anti-Sec5-RBD antibody abolished the interaction between Ral and Exo84.

An increase in intracellular Ca^{2+} concentration is the trigger for regulated exocytosis in many cell types, including platelets (1, 5, 6). Therefore, we examined the role of Ral on the Ca^{2+}-induced secretion from permeabilized platelets. The amount of secretion increased with increasing Ca^{2+} concentration (*closed squares* in Fig. 6), and the addition of Sec5-RBD alone did not inhibit the secretion (*open squares* in Fig. 6). However, this result did not imply that Ral was not involved in platelet dense granule secretion under physiological conditions because increased Ca^{2+} concentration alone did not induce Ral activation without the addition of non-hydrolyzable GTP analogues in permeabilized platelets (data not shown). GppNHp shifted the Ca^{2+} concentration-response curve for dense granule secretion to the left (*closed circles* in Fig. 6), indicating that GppNHp increased the Ca^{2+} sensitivity of the secretion as shown previously (7). The addition of Sec5-RBD inhibited this enhancement by GppNHp (*open circles* in Fig. 6). Thus, we conclude that Ral could regulate the Ca^{2+} sensitivity of platelet dense granule secretion. In other words, Ral could increase the efficiency of exocytosis in response to low levels of intracellular Ca^{2+} signals.

The intracellular Ca^{2+} concentration measured by fluorescence indicators is typically in the range of 40 to 80 nM in resting platelets (5). Real-time monitoring of intracellular Ca^{2+} concentrations of platelets by confocal imaging technique under flow condition revealed that intracellular Ca^{2+} concentrations vary considerably, ranging from 0.2 to 2 μM during thrombus formation, and the concentration is below 1 μM in many platelets (3). Thus, it is conceivable that the Ral-exocyst pathway could contribute to the regulation of dense granule secretion in such submaximally activated platelets. Ral is abundant in platelets (20, 21) and is rapidly activated by agonist stimulation in intact platelets (17). Furthermore, thrombin stimulation induced the association of Ral and the exocyst complex in intact platelets (Fig. 7*D*). These observations also support the idea that the Ral-exocyst pathway plays an important role in regulated exocytosis in platelets in certain physiological conditions.

The exocyst complex has been demonstrated to be involved in constitutive exocytosis, such as polarized delivery of membrane proteins to the basolateral surface in epithelial cells (31) and delivery of glutamate receptors to the postsynaptic membrane in neurons (47, 48). On the other hand, there have been only a few reports showing the involvement of the exocyst complex in regulated exocytosis. Inoue *et al.* (33, 34) have reported that Exo70, a component of the exocyst complex, binds the Rho family GTPase TC10 and plays a role in the targeting of glucose transporter 4 to the plasma membrane in insulin-stimulated adipocytes. Tsuboi *et al.* (49) have shown that the exocyst complex serves to regulate the docking of insulin-containing vesicles at sites of release in response to glucose stimulation in pancreatic β cells, although the involvement of a small GTPase regulating the exocyst complex remains to be determined. In this study, we provided the evidence that the exocyst complex and Ral GTPase could control regulated exocytosis of platelet dense granules by increasing the Ca^{2+} sensitivity of exocytosis. It will be important to elucidate the mechanism of how the Ral-exocyst pathway functions in regulated exocytosis, especially in the regulation of the Ca^{2+} sensitivity of secretion.

Acknowledgments—We thank the Kyoto Red Cross Blood Center for providing platelet pellets. We also thank Tomoko Matsubara for excellent technical assistance.

REFERENCES

1. Offermanns, S. (2006) *Circ. Res.* **99,** 1293–1304
2. Horiuchi, H. (2006) *Ann. Med.* **38,** 162–172
3. Nesbitt, W. S., Giuliano, S., Kulkarni, S., Dopheide, S. M., Harper, I. S., and Jackson, S. P. (2003) *J. Cell Biol.* **160,** 1151–1161
4. Brass, L. F. (2005) in *Hematology: The Molecular Basis for Platelet Activation* (Hoffman, R., Benz, E. J., Jr., Shattil, S. J., Furie, B., Cohen, H. J., Silberstein, L. E., and McGlave, P., eds) 4th Ed., pp. 1889–1914, Elsevier, New York
5. Sargeant, P., and Sage, S. O. (1994) *Pharmacol. Ther.* **64,** 395–443
6. Burgoyne, R. D., and Morgan, A. (2003) *Physiol. Rev.* **83,** 581–632
7. Haslam, R. J., and Davidson, M. M. (1984) *FEBS Lett.* **174,** 90–95
8. Haslam, R. J., and Davidson, M. M. (1984) *J. Recept. Res.* **4,** 605–629
9. Haslam, R. J., and Davidson, M. M. (1985) *Nature* **313,** 821–822
10. Coorssen, J. R., Davidson, M. M., and Haslam, R. J. (1990) *Cell Regul.* **1,** 1027–1041
11. Padfield, P. J., Panesar, N., Henderson, P., and Baldassare, J. J. (1996) *Biochem. J.* **314,** 123–128
12. Takai, Y., Sasaki, T., and Matozaki, T. (2001) *Physiol. Rev.* **81,** 153–208
13. Wennerberg, K., Rossman, K. L., and Der, C. J. (2005) *J. Cell Sci.* **118,** 843–846
14. Wolthuis, R. M., Zwartkruis, F., Moen, T. C., and Bos, J. L. (1998) *Curr. Biol.* **8,** 471–474
15. Bos, J. L. (1998) *EMBO J.* **17,** 6776–6782
16. Hofer, F., Berdeaux, R., and Martin, G. S. (1998) *Curr. Biol.* **8,** 839–842
17. Wolthuis, R. M., Franke, B., van Triest, M., Bauer, B., Cool, R. H., Camonis, J. H., Akkerman, J. W., and Bos, J. L. (1998) *Mol. Cell. Biol.* **18,** 2486–2491
18. Feig, L. A. (2003) *Trends Cell Biol.* **13,** 419–425
19. van Dam, E. M., and Robinson, P. J. (2006) *Int. J. Biochem. Cell Biol.* **38,** 1841–1847
20. Bhullar, R. P., Chardin, P., and Haslam, R. J. (1990) *FEBS Lett.* **260,** 48–52
21. Bhullar, R. P., and Yang, S. (1998) *Mol. Cell. Biochem.* **179,** 49–55
22. Mark, B. L., Iilkina, O., and Bhullar, R. P. (1996) *Biochem. Biophys. Res. Commun.* **225,** 40–46
23. Lipschutz, J. H., and Mostov, K. E. (2002) *Curr. Biol.* **12,** R212–214
24. Brymora, A., Valova, V. A., Larsen, M. R., Roufogalis, B. D., and Robinson, P. J. (2001) *J. Biol. Chem.* **276,** 29792–29797
25. Moskalenko, S., Henry, D. O., Rosse, C., Mirey, G., Camonis, J. H., and White, M. A. (2002) *Nat. Cell Biol.* **4,** 66–72
26. Sugihara, K., Asano, S., Tanaka, K., Iwamatsu, A., Okawa, K., and Ohta, Y. (2002) *Nat. Cell Biol.* **4,** 73–78
27. Moskalenko, S., Tong, C., Rosse, C., Mirey, G., Formstecher, E., Daviet, L., Camonis, J., and White, M. A. (2003) *J. Biol. Chem.* **278,** 51743–51748
28. Jin, R., Junutula, J. R., Matern, H. T., Ervin, K. E., Scheller, R. H., and Brunger, A. T. (2005) *EMBO J.* **24,** 2064–2074
29. TerBush, D. R., Maurice, T., Roth, D., and Novick, P. (1996) *EMBO J.* **15,** 6483–6494
30. Guo, W., Roth, D., Walch-Solimena, C., and Novick, P. (1999) *EMBO J.* **18,** 1071–1080
31. Grindstaff, K. K., Yeaman, C., Anandasabapathy, N., Hsu, S. C., Rodriguez-Boulan, E., Scheller, R. H., and Nelson, W. J. (1998) *Cell* **93,** 731–740
32. Shipitsin, M., and Feig, L. A. (2004) *Mol. Cell. Biol.* **24,** 5746–5756
33. Inoue, M., Chang, L., Hwang, J., Chiang, S. H., and Saltiel, A. R. (2003) *Nature* **422,** 629–633
34. Inoue, M., Chiang, S. H., Chang, L., Chen, X. W., and Saltiel, A. R. (2006) *Mol. Biol. Cell* **17,** 2303–2311

35. Fukai, S., Matern, H. T., Jagath, J. R., Scheller, R. H., and Brunger, A. T. (2003) *EMBO J.* **22,** 3267–3278
36. Palmer, M., Harris, R., Freytag, C., Kehoe, M., Tranum-Jensen, I., and Bhakdi, S. (1998) *EMBO J.* **17,** 1598–1605
37. Shirakawa, R., Yoshioka, A., Horiuchi, H., Nishioka, H., Tabuchi, A., and Kita, T. (2000) *J. Biol. Chem.* **275,** 33844–33849
38. Yoshioka, A., Shirakawa, R., Nishioka, H., Tabuchi, A., Higashi, T., Ozaki, H., Yamamoto, A., Kita, T., and Horiuchi, H. (2001) *J. Biol. Chem.* **276,** 39379–39385
39. Shirakawa, R., Higashi, T., Tabuchi, A., Yoshioka, A., Nishioka, H., Fukuda, M., Kita, T., and Horiuchi, H. (2004) *J. Biol. Chem.* **279,** 10730–10737
40. Shirakawa, R., Higashi, T., Kondo, H., Yoshioka, A., Kita, T., and Horiuchi, H. (2005) *Methods Enzymol.* **403,** 778–788
41. Kondo, H., Shirakawa, R., Higashi, T., Kawato, M., Fukuda, M., Kita, T., and Horiuchi, H. (2006) *J. Biol. Chem.* **281,** 28657–28665
42. Fabiato, A., and Fabiato, F. (1979) *J. Physiol. (Paris)* **75,** 463–505
43. Christoforidis, S., McBride, H. M., Burgoyne, R. D., and Zerial, M. (1999) *Nature* **397,** 621–625
44. Nishi, E., Hiraoka, Y., Yoshida, K., Okawa, K., and Kita, T. (2006) *J. Biol. Chem.* **281,** 31164–31172
45. Yoshioka, A., Horiuchi, H., Shirakawa, R., Nishioka, H., Tabuchi, A., Higashi, T., Yamamoto, A., and Kita, T. (2001) *Ann. N. Y. Acad. Sci.* **947,** 403–406
46. Wang, L., Li, G., and Sugita, S. (2004) *J. Biol. Chem.* **279,** 19875–19881
47. Sans, N., Prybylowski, K., Petralia, R. S., Chang, K., Wang, Y. X., Racca, C., Vicini, S., and Wenthold, R. J. (2003) *Nat. Cell Biol.* **5,** 520–530
48. Gerges, N. Z., Backos, D. S., Rupasinghe, C. N., Spaller, M. R., and Esteban, J. A. (2006) *EMBO J.* **25,** 1623–1634
49. Tsuboi, T., Ravier, M. A., Xie, H., Ewart, M. A., Gould, G. W., Baldwin, S. A., and Rutter, G. A. (2005) *J. Biol. Chem.* **280,** 25565–25570

ATH-10228; No. of Pages 8

ELSEVIER

Atherosclerosis xxx (2008) xxx–xxx

ATHEROSCLEROSIS

www.elsevier.com/locate/atherosclerosis

Lectin-like oxidized LDL receptor-1 (LOX-1) acts as a receptor for remnant-like lipoprotein particles (RLPs) and mediates RLP-induced migration of vascular smooth muscle cells

Yo Aramaki [b], Hirokazu Mitsuoka [a], Masako Toyohara [a], Toshikazu Jinnai [a], Kazushi Kanatani [c], Katsuyuki Nakajima [c], Eri Mukai [b], Yuichiro Yamada [b,d], Toru Kita [a], Nobuya Inagaki [b], Noriaki Kume [a,*]

[a] *Department of Cardiovascular Medicine, Graduate School of Medicine, Kyoto University, Japan*
[b] *Department of Diabetes and Clinical Nutrition, Graduate School of Medicine, Kyoto University, Japan*
[c] *JIMRO, Co Ltd, Japan*
[d] *Divison of Endocrinology, Diabetes and Geriatric Medicine, Department of Internal Medicine, Akita University School of Medicine, 1-1-1 Hondo, Akita 010-8543, Japan*

Received 22 March 2007; received in revised form 5 December 2007; accepted 15 December 2007

Abstract

Objective: Remnant-like lipoprotein particles (RLPs) have been implicated in atherogenesis especially by diabetic dyslipidemia; however, their receptor(s) and effects on vascular smooth muscle cells (VSMCs) remain unclear. In this study, we examined if lectin-like oxidized LDL receptor-1 (LOX-1) acts as a receptor for RLPs and its biological effects in VSMCs.

Methods and results: RLPs were isolated from human plasma by immunoaffinity gel containing anti-apolipoprotein A-I and anti-apolipoprotein B-100 monoclonal antibodies. DiI-labeled RLPs were taken up by CHO-K1 cells stably expressing LOX-1 but not by wild-type CHO-K1 cells. RLPs induced LOX-1 expression and cell migration in bovine VSMCs (BVSMCs), which were significantly suppressed by transfection with LOX-1 specific siRNAs. Inhibitors of metalloproteinases, epidermal growth factor (EGF) receptor tyrosine kinase, heparin-binding EGF-like growth factor (HB-EGF), p38 mitogen-activated protein kinase (p38 MAPK), MAPK kinase (MEK1) and phosphoinositide 3-kinase (PI3K) significantly blocked RLP-induced LOX-1 expression and cell migration of BVSMCs.

Conclusions: The present study provides direct evidence that LOX-1 is a novel receptor for RLPs in VSMCs. LOX-1-mediated uptake of RLPs may thus play important roles in atherogenesis by inducing LOX-1 expression and VSMC migration especially in the settings of postprandial hyperlipidemia, diabetes and metabolic syndrome.

Keywords: LOX-1; Atherosclerosis; Remnant lipoproteins; Vascular smooth muscle; Diabetes mellitus

1. Introduction

Coronary heart disease (CHD) is prevalent in diabetes mellitus and metabolic syndrome [1,2], in which plasma lipoprotein profiles are characterized by elevated remnant lipoprotein levels. Plasma remnant lipoprotein levels have been assessed as levels of remnant-like lipoprotein particles (RLPs) by isolating fractions unbound to two monocolonal antibodies directed to apolipoprotein B-100 and apolipoprotein A-I [3]. By this method, plasma RLP levels have been shown to predict the CHD risk [4–7], and also to have biological effects on macrophages and vascular cells related to atherogenesis [8–11].

Vascular smooth muscle cells (VSMCs) migration from media to intima and subsequent proliferation play key roles in atherogenesis [12]. A previous report has demonstrated

* Corresponding author at: Department of Cardiovascular Medicine, Graduate School of Medicine, Kyoto University, 54 Kawahara-cho, Shogoin, Sakyo-ku, Kyoto 606-8507, Japan. Tel.: +81 75 751 3623; fax: +81 75 751 4094.
E-mail address: nkume@kuhp.kyoto-u.ac.jp (N. Kume).

0021-9150/$ – see front matter © 2008 Elsevier Ireland Ltd. All rights reserved.
doi:10.1016/j.atherosclerosis.2007.12.017

Please cite this article in press as: Aramaki Y, et al., Lectin-like oxidized LDL receptor-1 (LOX-1) acts as a receptor for remnant-like lipoprotein particles (RLPs) and mediates RLP-induced migration of vascular smooth muscle cells, Atherosclerosis (2008), doi:10.1016/j.atherosclerosis.2007.12.017

that RLPs induce VSMC proliferation [9]; however, their effects on VSMC migration have not been clarified. In addition, receptors for RLPs in VSMCs have not yet been well characterized, although LRP in the liver [13], apoB-48-R in macrophages [10,14], and VLDL receptor in heart, skeletal muscle, adipose tissue, brain and macrophages [15] have been shown to act as a receptor for RLPs.

Lectin-like oxidized LDL receptor-1 (LOX-1) is a receptor for Ox-LDL expressed in vascular endothelial cells, macrophages and VSMCs [16–21]. LOX-1 expression is dynamically inducible by various proatherogenic stimuli, including tumor necrosis factor-α (TNF-α) [18,21], heparin-binding epidermal growth factor-like growth factor (HB-EGF), [22] and Ox-LDL [23]. Furthermore, LOX-1 is highly expressed by macrophages and VSMCs accumulated in the intima of advanced atherosclerotic lesions, as well as endothelial cells covering early atherosclerotic lesions in vivo [24], indicating that LOX-1 appears to play important roles at various stages of atherogenesis.

In previous reports, LOX-1 has been indicated to act as a receptor for RLPs in vascular endothelial cells using an anti-LOX-1 antibody and an antisense oligonucleotide directed to LOX-1 [25,26]. In the present study, we provide direct evidence, by cDNA and short interference RNAs (siRNAs) transfection, that LOX-1 acts as a receptor for RLP and whereby induce VSMC migration, depending upon HB-EGF shedding and the downstream signal transduction cascades.

2. Materials and methods

2.1. Reagents

AG1478, PD98059, SB203580 and wortmannin were purchased from Calbiochem (San Diego, CA). CRM197 was from Sigma Chemical CO (St. Louis, MO). GM6001 and its negative control compound were from Chemicon (Temecula, CA). PDGF-BB and TNF-α were purchased from Roche (Mannheim, Germany).

2.2. Cell culture

Chinese hamster ovary-K1 (CHO-K1) cells stably expressing human LOX-1 (hLOX-1-CHO) or bovine LOX-1 (bLOX-1-CHO), as well as wild-type CHO-K1 cells (wt-CHO), were established and cultured as previously reported [16,17]. Bovine VSMCs (BVSMCs) were purchased from Cell Applications, Inc. (San Diego, CA) and cultured as previously reported [19,22].

2.3. Antibodies

Mouse anti-bovine LOX-1 and anti-human LOX-1 monoclonal antibodies were prepared by immunization with recombinant bovine and human LOX-1 extracelluler domains as previously described [16]. Polyclonal antibodies for phosphorylated and total SAPK/JNK and p38 MAPK were purchased from Cell Signaling Technology (New England Biolabs, London, UK). Polyclonal antibodies for phosphorylated and total ERK, Akt and EGFR were from Santa Cruz Biotechnology (Santa Cruz, CA).

2.4. Lipoprotein preparation

RLPs and nascent VLDL were separated using an immunoaffinity mixed gel (JIMRO, Gunma, Japan) from triglyceride-rich lipoprotein fraction ($d < 1.006$ g/ml) isolated from human plasma using ultracentrifugation as described previously [3]. LDL fraction ($d = 1.019–1.063$ g/ml) was also isolated and modified oxidatively as previously described [16,17,19]. Lipoproteins were dialyzed overnight against PBS containing 1 mM EDTA (pH 7.4) and sterilized with a 0.22-μm filter unit (Millipore, Billerica, MA). Labeling of lipoproteins with 1,1′-dioctadecyl-3,3,3′,3′-tetramethylindocarbocyanine perchlorate (DiI; Molecular Probes, Eugene, OR) and quantification of DiI-labeled lipoprotein uptake were performed as previously described [16].

2.5. Immunoblot analysis

Total cell lysates were separated on 12% SDS-PAGE, transferred onto nitrocellulose membranes (Schleicher & Schuell, Dassel, Germany) and proved with each primary antibody, horseradish peroxidase-linked secondary antibodies (Amersham, Hilleroed, Denmark) and the ECL Western blotting detection reagents (Amersham). Representative results from three independent experiments are shown in figures.

2.6. Northern blot analysis

Total cellular RNA was isolated by RNeasy Plus Mini Kit (Qiagen, Valencia, CA). Total RNA (15 μg) was subjected to electrophoresis through 1% agarose gels containing formaldehyde, and transferred onto nitrocellulose membranes (OPTITRAN, Schleicher & Schuell). Membranes were hybridized with XhoI fragment of bovine LOX-1 cDNA which had been labeled with [α-^{32}P] dCTP (Amersham) using random oligonucleotide primers (Megaprime DNA labelling systems, Amersham).

2.7. Transwell migration assay

Transwell migration assay was performed as previously described [27,28]. BVSMCs were applied to the upper chamber of transwell (Costar, Corning Inc. Corning, NY) containing serum-free medium and allowed to migrate to lower chamber containing test stimuli through a fibronectin-coated polycarbonate filter (8 μm pore). Migrated cells on the bottom side of filter were fixed with 100% methanol, stained with Harris hematoxylin solution, and counted manually in randomly chosen five high power fields in each tran-

Please cite this article in press as: Aramaki Y, et al., Lectin-like oxidized LDL receptor-1 (LOX-1) acts as a receptor for remnant-like lipoprotein particles (RLPs) and mediates RLP-induced migration of vascular smooth muscle cells, Atherosclerosis (2008), doi:10.1016/j.atherosclerosis.2007.12.017

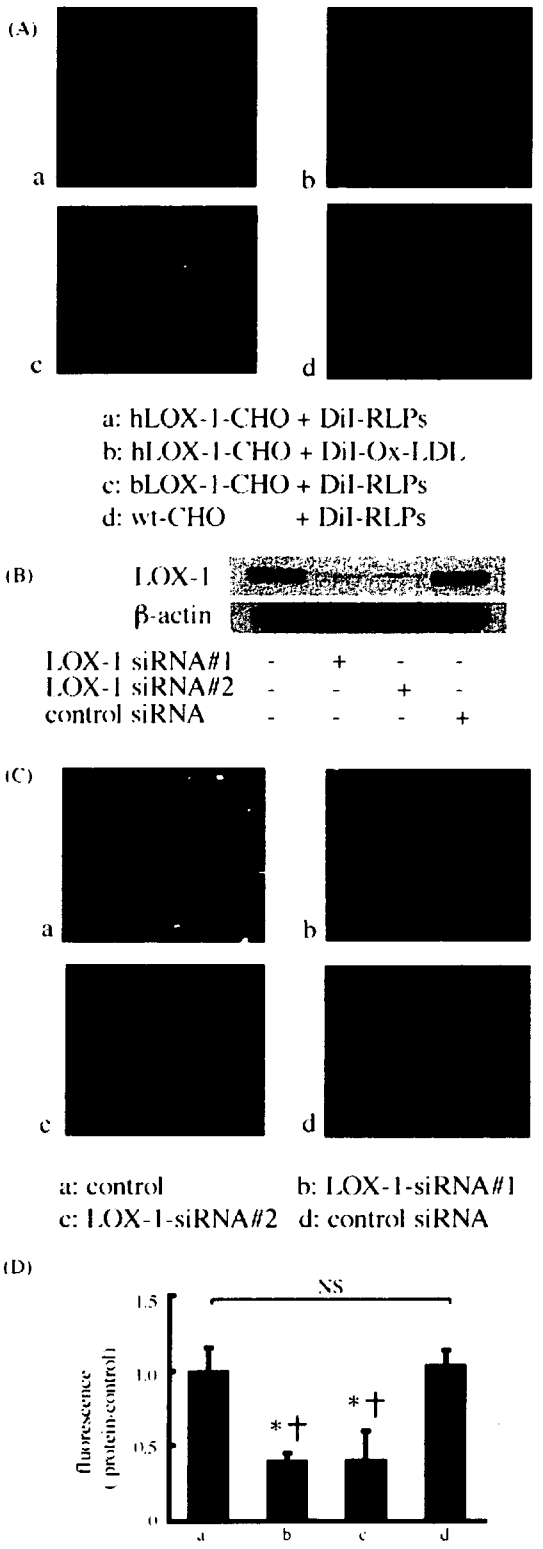

Fig. 1. Human and bovine LOX-1 mediates uptake of RLPs. (A) hLOX-1-CHO were incubated with 5 μg/ml of DiI-RLPs (a) or DiI-labeled Ox-LDL (b) for 2 h. bLOX-1-CHO (c) as well as wt-CHO (d) were incubated with 5 μg/ml of DiI-RLPs. (B) Total cell lysates of bLOX-1-CHO transfected with or without 100 nM of LOX-1 siRNA #1, #2 or control non-silencing siRNA (control siRNA) were subjected to Western blotting for LOX-1. (C) BVSMCs transfected with or without (a) 100 nM of LOX-1 siRNA#1 (b), #2 (c) or control siRNA (d) were incubated with 5 μg/ml of DiI-RLPs. Representative pictures under fluorescence microscopy are shown. (D) Uptake of DiI-RLPs was quantified by measuring fluorescence counts after extraction of DiI. (*) $p < 0.0001$ vs. control, (†) $p < 0.0001$ vs. control siRNA.

swell, using a light microscope (Axioskop2 plus, Zeiss, Jena, Germany). Relative average numbers of migrated BVSMCs compared with the control were calculated.

2.8. LOX-1 specific short interference RNAs (siRNAs)

To block bovine LOX-1 expression, we designed two different siRNAs directed to the coding sequence of bovine LOX-1; siRNA #1: ACCCAAUUACUCGUGGCUU (650-668) and siRNA #2: GGCGAAUCUAUUGAGAGCA (821-839). None of these siRNAs shares homology with exons of other known bovine genes. Control non-silencing siRNA (control siRNA) was obtained from Qiagen. For siRNA transfection, bLOX-1-CHO and BVSMCs were transfected with siRNAs using siFECTOR (B-Bridge International, Inc. Mountain View, CA) according to the manufacturer's instructions.

2.9. Statistical analysis

Data in the bar graphs indicate the mean ± S.D. calculated from three independent experiments. One-way ANOVA was used to compare differences among groups. Statistical significance was defined as $p < 0.05$.

3. Results

3.1. Uptake of DiI-labeled RLPs in CHO-K1 cells stably expressing LOX-1

To examine whether LOX-1 acts as a receptor for RLPs, hLOX-1-CHO, bLOX-1-CHO and wt-CHO were incubated with DiI-labeled RLPs (DiI-RLPs) or DiI-Ox-LDL. As shown in Fig. 1A, hLOX-1-CHO, but not wt-CHO, showed prominent uptake of DiI-RLPs as well as DiI-Ox-LDL. Uptake of DiI-RLP in hLOX-1-CHO was competitively inhibited by the 100-fold excess amount of unlabeled RLPs or Ox-LDL (data not shown), suggesting that uptake of RLPs is specific and that binding sites for RLPs and Ox-LDL on the LOX-1 molecule are identical or overlapped. DiI-RLPs, as well as DiI-Ox-LDL, were also taken up by bLOX-1-CHO. These results thus demonstrate that both human and bovine LOX-1 act as receptors for RLPs.

3.2. Uptake of RLPs by BVSMCs is significantly suppressed by transfection with LOX-1 specific siRNAs

We confirmed that both of LOX-1 siRNA #1 and #2, but not control siRNA, dramatically reduce LOX-1 expression in

Please cite this article in press as: Aramaki Y, et al., Lectin-like oxidized LDL receptor-1 (LOX-1) acts as a receptor for remnant-like lipoprotein particles (RLPs) and mediates RLP-induced migration of vascular smooth muscle cells, Atherosclerosis (2008), doi:10.1016/j.atherosclerosis.2007.12.017

bLOX-1-CHO or BVSMCs by more than 90% (Fig. 1B). To determine whether RLPs are mainly taken up by BVSMCs via LOX-1, BVSMCs were incubated with DiI-RLPs after transfection with LOX-1 siRNAs or control siRNA. Uptake of RLPs was significantly reduced in BVSMCs transfected with LOX-1 siRNAs when compared to those transfected with control siRNA or without siRNA (Fig. 1C and D), indicating that LOX-1 is one of major receptors for RLPs in BVSMCs.

3.3. RLPs induce LOX-1 expression in BVSMCs

To explore biological effects of RLPs on BVSMCs, LOX-1 expression was evaluated by Western blotting. As shown in Fig. 2A, treatment of BVSMCs with RLPs, as well as TNF-α, significantly increased LOX-1 expression in a concentration-dependent fashion; maximal effects were observed at 25–50 μg/ml of RLPs. Time-course experiments showed that expression of LOX-1 peaked at 16–20 h after RLP treatment and declined after 24 h (Fig. 2B). Furthermore, Northern blot analyses show RLPs induced LOX-1 expression at the level of gene transcription (Fig. 2C). In contrast with RLPs, nascent VLDL (n-VLDL) had negligible effects on LOX-1 expression in BVSMCs (supplemental Fig. S-A).

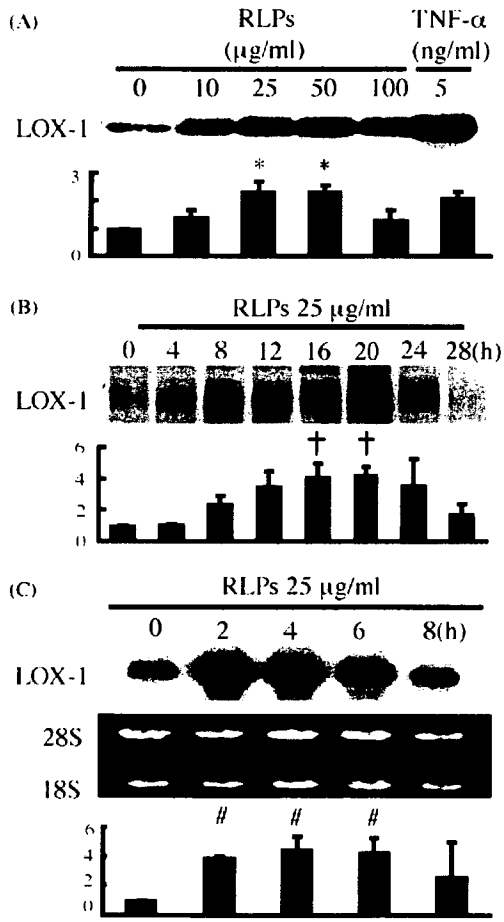

Fig. 2. RLPs, but not nascent VLDL (n-VLDL), induce LOX-1 expression in BVSMCs. (A and B) After BVSMCs were treated with the indicated concentrations of RLPs for 16 h (A) or 25 μg/ml of RLPs for the indicated time periods (B), total cell lysates were subjected to immunoblotting for LOX-1. TNF-α served as a positive control. (C) After treatment with 25 μg/ml of RLPs for the indicated time periods, total cellular RNA was subjected to Northern blot analyses. Bands for 28S and 18S ribosomal RNAs were visualized by ethidium bromide staining to control the amount of RNA loaded. (*) $p < 0.001$ vs. 0 μg/ml of RLPs, (†) $p < 0.005$ vs. 0 h-incubation, (#) $p < 0.05$ vs. 0 h-incubation.

3.4. RLPs induce migration of BVSMCs via LOX-1

Effects of RLPs on BVSMC migration were examined by a transwell migration assay. As shown in Fig. 3A and B, RLPs, as well as PDGF-BB, significantly enhanced BVSMC migration compared with control in serum-free media. N-VLDL showed modest and statistically insignificant increases in BVSMC migration. Statistically significant increases in cell migration were observed at 25 and 50 μg/ml of RLPs after the stimulation for more than 8 h (supplemental Fig. S-B). BVSMC migration was not enhanced when RLPs were present both in the upper and lower chambers, as compared with that without RLPs (supplemental Fig. S-C). Therefore, the increases in the cell numbers on the bottom sides of the filters were due to chemotaxis or cell migration rather than chemokinesis or cell proliferation. Fig. 3C shows that RLP-induced BVSMC migration, but not PDGF-BB-induced BVSMC migration, was significantly inhibited by LOX-1 siRNA transfection. These results indicate LOX-1 mediates RLP-induced BVSMC migration.

3.5. RLP-induced expression of LOX-1 depends upon HB-EGF shedding and EGFR phosphorylation

A previous study has shown that RLPs induce proliferation of rat VSMCs via shedding of HB-EGF and subsequent EGFR transactivation [9], we sought to determine if RLP-induced LOX-1 expression depends upon HB-EGF shedding and EGFR transactivation. As shown in Fig. 4A, RLPs, but not n-VLDL, activate EGFR. In addition, CRM197, which functionally neutralizes HB-EGF, suppressed the activation of EGFR. Furthermore, a metalloproteinase inhibitor GM6001 (GM), but not its negative control compound (GMNC), significantly suppressed RLP-induced LOX-1 expression (Fig. 4B). In addition, AG1478, an EGFR tyrosine kinase inhibitor and CRM197 significantly inhibited LOX-1 expression induced by RLPs, respectively (Fig. 4C and D), indicating involvement of certain metalloproteinases, HB-EGF shedding and transactivation of EGFR in RLP-induced LOX-1 expression in BVSMCs.

3.6. RLP-induced expression of LOX-1 depends upon ERK, p38 MAPK and PI3K activation

To determine which signal transduction cascades are involved in RLP-induced LOX-1 expression in BVSMCs, phosphorylation of ERK, p38 MAPK, c-Jun N-terminal

Please cite this article in press as: Aramaki Y, et al., Lectin-like oxidized LDL receptor-1 (LOX-1) acts as a receptor for remnant-like lipoprotein particles (RLPs) and mediates RLP-induced migration of vascular smooth muscle cells, Atherosclerosis (2008), doi:10.1016/j.atherosclerosis.2007.12.017

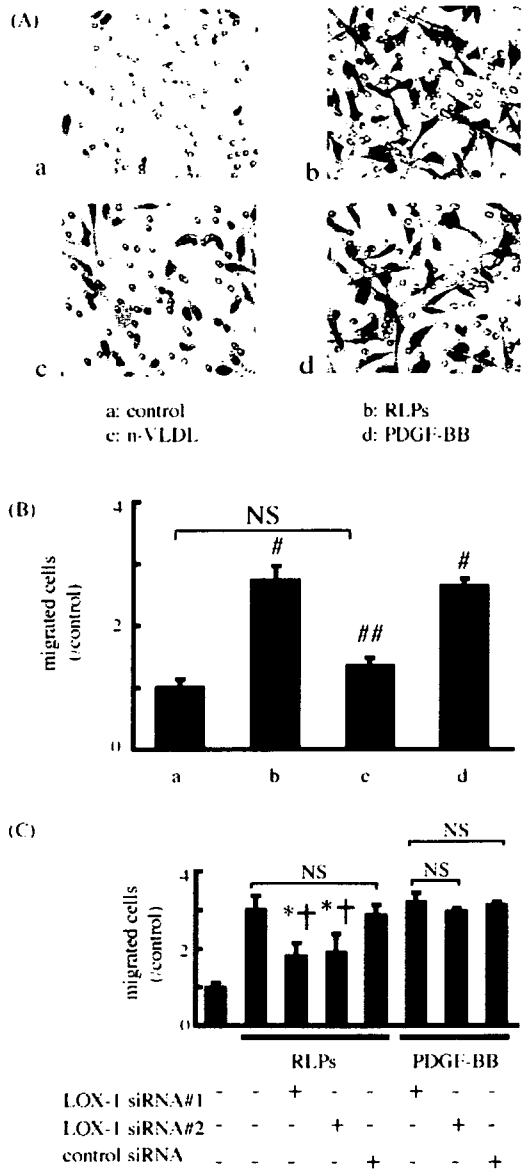

Fig. 3. LOX-1 mediates RLP-induced, but not PDGF-induced, BVSMC migration. (A and B) BVSMCs were applied to the upper chamber of transwells whose lower chamber contained serum-free medium with or without (a), RLPs (25 μg/ml; b), n-VLDL (25 μg/ml; c), or PDGF-BB (3 ng/ml; d). Representative photomicrographs (A) and migrated cell numbers (B) from three independent experiments are shown (A). (C) After transfection with or without 100 nM of LOX-1 siRNA #1, LOX-1 siRNA #2, or control siRNA, BVSMCs were subjected to the transwell cell migration assay with RLPs (25 μg/ml) or PDGF-BB (3 ng/ml) for 8 h. (#) $p < 0.0001$ vs. control, (##) $p < 0.005$ vs. RLPs, (*) $p < 0.05$ vs. RLPs without siRNAs. (†) $p < 0.05$ vs. RLPs with control siRNA.

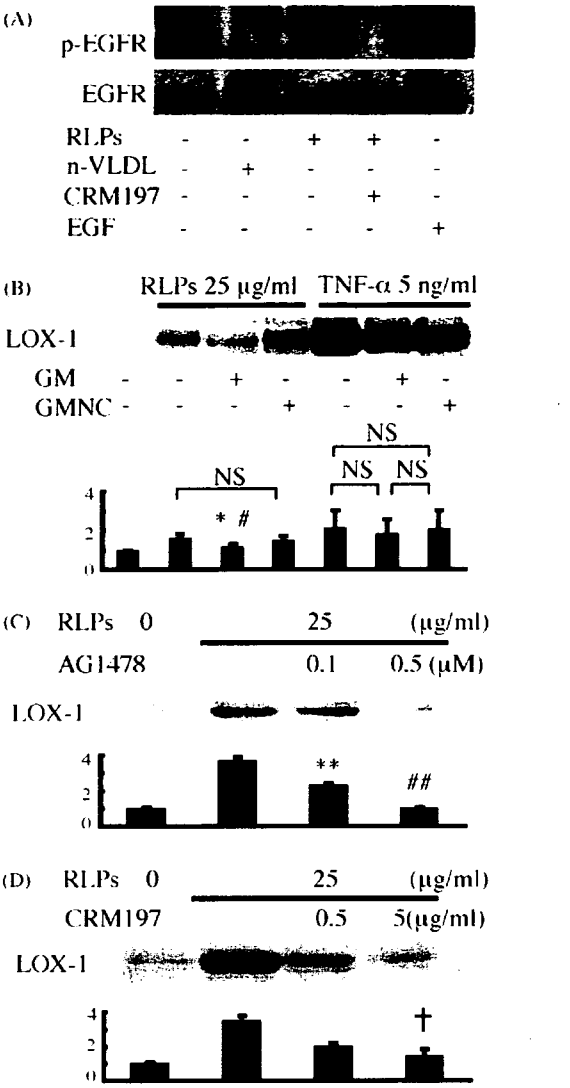

Fig. 4. Phosphorylation of EGFR induced by RLPs, and involvement of metalloproteinase activation, HB-EGF shedding and EGFR transactivation in RLP-induced LOX-1 expression. (A) BVSMCs were incubated with 25 μg/ml RLPs with or without 1 h-pretreatment with CRM197 (5 μg/ml), 25 μg/ml of n-VLDL, or 10 ng/ml of EGF for 5 min. Then, total cell lysates were subjected to immunoblotting for phosphorylated or total EGFR. (B–D) After pretreated with 50 μM of GM or GMNC for 12 h (B), or with the indicated concentrations of AG1478 (C) or CRM197 (D) for 1 h, BVSMCs were incubated with RLPs or TNF-α for 16 h. Total cell lysates were subjected to immunoblot analyses for LOX-1. (*) $p < 0.05$ vs. RLPs without inhibitors, (#) $p < 0.05$ vs. RLPs with GMNC, (**) $p < 0.01$ and (##) $p < 0.001$ vs. RLPs without AG1478, (†) $p < 0.05$ vs. RLPs without CRM197.

kinase (JNK) and Akt elicited by RLPs were measured by immunoblotting. RLPs induced significant phosphorylation of ERK, p38 MAPK and Akt (Fig. 5A), but not JNK (data not shown). Furthermore, CRM197 significantly suppressed RLP-induced phosphorylation of these signals (data not shown). Dependency of RLP-induced LOX-1 expression upon ERK, p38 MAPK and PI3K was examined by specific inhibitors. As shown in Fig. 5B, PD98059, SB203580 and wortmannin, an inhibitor of MEK1, p38 MAPK and phosphoinositide 3-kinase (PI3K), respectively, significantly suppressed RLP-induced LOX-1 expression in BVSMC. These results indicate RLP-induced LOX-1 expression depends upon MEK1-ERK, p38 MAPK and PI3K-Akt cascades located downstream to the EGFR transactivation, respectively.

Please cite this article in press as: Aramaki Y, et al., Lectin-like oxidized LDL receptor-1 (LOX-1) acts as a receptor for remnant-like lipoprotein particles (RLPs) and mediates RLP-induced migration of vascular smooth muscle cells, Atherosclerosis (2008), doi:10.1016/j.atherosclerosis.2007.12.017

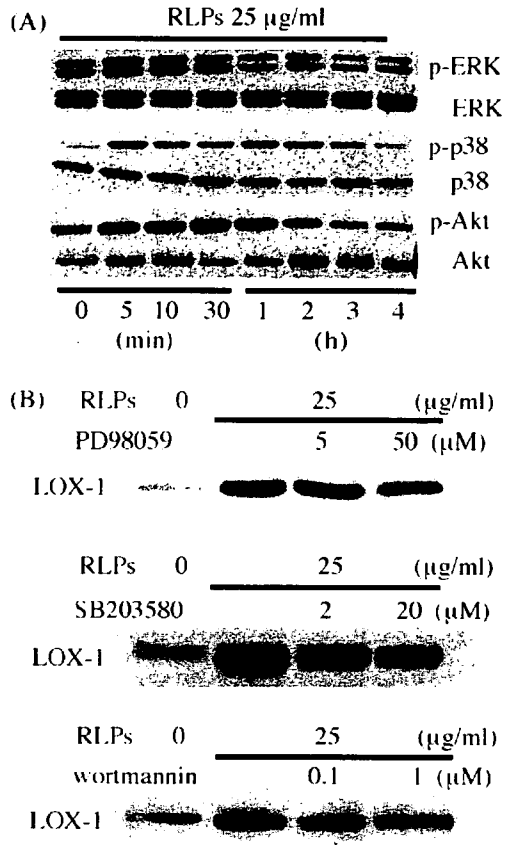

Fig. 5. Involvement of ERK, p38 MAPK and Akt phosphorylation in RLP-induced LOX-1 expression in BVSMCs. (A) After BVSMCs were incubated with 25 μg/ml of RLPs for the indicated periods, total cell lysates were subjected to immunoblot analyses for phosphorylated or total ERK, p38 MAPK and Akt. (B) After pretreated with the indicated concentrations of PD98059, SB203580 or wortmannin for 1 h, BVSMCs were incubated with RLPs (25 μg/ml) for 16 h and then subjected to immunoblotting for LOX-1.

3.7. Shedding of HB-EGF, EGFR transactivation and phosphorylation of ERK, p38 MAPK and Akt are involved in RLP-induced cell migration of BVSMCs

Pretreatment with GM, AG1478 and CRM197, but not GMNC, significantly suppressed RLP-induced VSMC migration (Fig. 6A and B). Furthermore, PD98059, SB203580 and wortmannin significantly suppressed migration of BVSMCs induced by RLPs (Fig. 6C). These results indicate RLP-induced BVSMC migration depends upon HB-EGF shedding, EGFR transactivation, and subsequent activation of MEK1-ERK, p38 MAPK and PI3K-Akt.

4. Discussion

In this study, we have provided the direct evidences that LOX-1 serves as a receptor for RLPs in VSMCs by use of two cell lines which stably express human or bovine LOX-1 and siRNA directed to LOX-1. In addition, we have shown

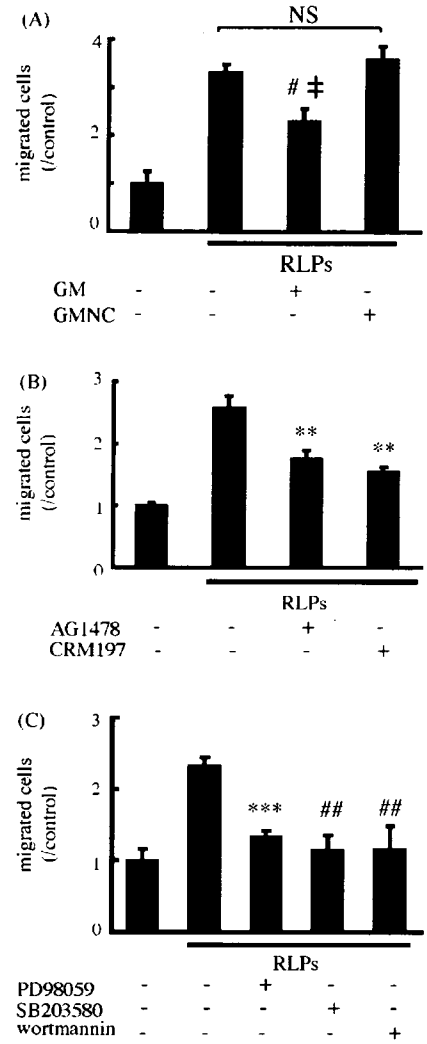

Fig. 6. Involvement of metalloproteinase activation, HB-EGF shedding, EGFR transactivation, and activation of ERK, p38 MAPK and PI3K in RLP-induced migration of BVSMCs. (A–C) After pretreatment with 50 μM of GM or GMNC for 12 h (A), AG1478 (0.5 μM) or CRM197 (5 μg/ml) for 1 h (B), or with PD98059 (50 μM), SB203580 (20 μM), or wortmannin (1 μM) for 1 h (C), BVSMCs were subjected to cell migration assay with RLPs (25 μg/ml) for 8 h. (#) $p < 0.005$ vs. RLPs without inhibitors, (‡) $p < 0.005$ vs. GMNC, (**) $p < 0.0001$, (***) $p < 0.001$, (##) $p < 0.005$ vs. RLPs without inhibitors.

that RLPs induce cell migration and LOX-1 expression by RLP-LOX-1 interactions, thus making a positive-feed back loop to further enhance the RLP-induced vascular dysfunction, as we already showed in oxidized LDL-induced vascular dysfunction [19].

In accordance with a previous report [9], we have demonstrated that RLP-induced LOX-1 expression and cell migration depend upon HB-EGF shedding and subsequent EGFR transactivation. Furthermore, we have shown the involvement of ERK, p38 MAPK and Akt as signal transducrion cascades located downstream to the EGFR transactivation. Furthermore, JNK was not activated by RLPs or not involved in RLP-induced LOX-1 expression or cell

Please cite this article in press as: Aramaki Y, et al., Lectin-like oxidized LDL receptor-1 (LOX-1) acts as a receptor for remnant-like lipoprotein particles (RLPs) and mediates RLP-induced migration of vascular smooth muscle cells, Atherosclerosis (2008), doi:10.1016/j.atherosclerosis.2007.12.017

migration (data not shown), indicating the specificity of the RLP-induced signals.

Competition studies in cells stably expressing LOX-1 indicated binding site(s) on the LOX-1 molecule for RLPs and oxidized LDL appear to be identical or overlapped, suggesting the C-terminal cysteine-rich C-type lectin-like domain may also be the responsible binding site(s) for RLPs [29], although the direct evidence should be provided in the future. Furthermore, previous studies have indicated that ADAMs are proteases responsible for HB-EGF shedding [30]; therefore, ADAMs may be involved in RLP-induced HB-EGF shedding. However, it remains to be fully elucidated which molecular mechanisms are involved after RLP-LOX-1 interactions to activate ADAMs which shed HB-EGF.

In summary, RLP-induced LOX-1 expression and VSMC migration appear to be important in atherogenesis elicited by postprandial hyperlipidemia, diabetes mellitus and metabolic syndrome. The present study has suggested the importance of LOX-1 in RLP-induced atherogenesis, as well as that induced by oxidized LDL. Further studies in suitable animal models, as well as clinical studies, would further elucidate the roles of LOX-1 in this process.

Acknowledgments

This work has been supported by Grants-in-Aid for Scientific Research (16590880, 18590985) from the Japanese Ministry of Education, Science, Sports, and Culture, and a research grant from Yokoyama Foundation for Clinical Pharmacology. We thank Kyoto Red Cross Blood Center for gift of unused human plasma.

Appendix A. Supplementary data

Supplementary data associated with this article can be found, in the online version, at doi:10.1016/j.atherosclerosis.2007.12.017.

References

[1] Kannel WB, McGee DL. Diabetes and cardiovascular disease, the Framingham study. JAMA 1979;41:2035–8.
[2] Alexander CM, Landsman PB, Teutsch SM, Haffner SM. NECP-defined metabolic syndrome, diabetes, and prevalence of coronary heart disease among NHANES III participants age 50 year and older. Diabetes 2003;52:1210–4.
[3] Nakajima K, Saito T, Tamura A, et al. Cholesterol in remnant-like lipoproteins in human serum using monoclonal anti apo B-100 and anti apo A-1 immunoaffinity mixed gels. Clin Chim Acta 1993;223:53–71.
[4] Nakamura T, Kugiyama K. Triglycerides and remnant particles as risk factors for coronary artery disease. Curr Atheroscler Rep 2006;8:107–10.
[5] Fukushima H, Sugiyama S, Honda O, et al. Prognostic value of remnant-like lipoprotein particle levels in patients with coronary artery disease and type II diabetes mellitus. J Am Coll Cardiol 2004;43:2219–24.
[6] Masuoka H, Kamei S. Predictive value of remnant-like particle cholesterol as an indicator of coronary artery stenosis in patients with normal serum triglyceride levels. Intern Med 2000;39:540–6.
[7] Higashi K, Ito T, Nakajima K, et al. Remnant-like particles cholesterol is higher in diabetic patients with coronary artery disease. Metabolism 2001;50:1462–5.
[8] Kawakami A, Tanaka A, Nakajima K, Shimokado K, Yoshida M. Atorvastatin attenuates remnant lipoprotein-induced monocyte adhesion to vascular endothelium under flow conditions. Circ Res 2002;91:263–71.
[9] Kawakami A, Tanaka A, Chiba T, et al. Remnant lipoprotein-induced smooth muscle cell proliferation involves epidermal growth factor receptor transactivation. Circulation 2003;108:2679–88.
[10] Kawakami A, Tani M, Chiba T, et al. Pitavastatin inhibits remnant lipoprotein-induced macrophage foam cell formation through ApoB48 receptor-dependent mechanism. Arterioscler Thromb Vasc Biol 2005;25:424–9.
[11] Tomono S, Kawazu S, Kato N, et al. Uptake of remnant like particles (RLP) in diabetic patients from mouse peritoneal macrophages. J Atheroscler Thromb 1994;1:98–102.
[12] Ross R. Atherosclerosis—an inflammatory disease. N Engl J Med 1999;340:115–26.
[13] Hussain MM, Maxfield FR, Mas-Oliva J, et al. Clearance of chylomicron remnants by the low density lipoprotein receptor-related protein/alpha 2-macroglobulin receptor. J Biol Chem 1991;266:13936–40.
[14] Gianturco SH, Ramprasad MP, Song R, et al. Apolipoprotein B-48 or its apolipoprotein B-100 equivalent mediates the binding of triglyceride-rich lipoproteins to their unique human monocyte-macrophage receptor. Arterioscler Thromb Vasc Biol 1998;18:968–76.
[15] Takahashi S, Sakai J, Fujino T, et al. The very low-density lipoprotein (VLDL) receptor: characterization and functions as a peripheral lipoprotein receptor. J Atheroscler Thromb 2004;11:200–8.
[16] Sawamura T, Kume N, Aoyama T, et al. An endothelial receptor for oxidized low-density lipoprotein. Nature 1997;386:73–7.
[17] Moriwaki H, Kume N, Sawamura T, et al. Ligand specificity of LOX-1, a novel endothelial receptor for oxidized low density lipoprotein. Arterioscler Thromb Vasc Biol 1998;18:1541–7.
[18] Moriwaki H, Kume N, Kataoka H, et al. Expression of lectin-like oxidized low density lipoprotein receptor-1 in human and murine macrophages: upregulated expression by TNF-α. FEBS Lett 1998;440:29–32.
[19] Kataoka H, Kume N, Miyamoto S, et al. Oxidized LDL modulates Bax/Bcl-2 through the lectinlike Ox-LDL receptor-1 in vascular smooth muscle cells. Arterioscler Thromb Vasc Biol 2001;21:955–60.
[20] Kume N, Kita T. Apoptosis of vascular cells by oxidized LDL: involvement of caspases and LOX-1 and its implication in atherosclerotic plaque rupture. Circ Res 2004;94:269–70.
[21] Kume N, Murase T, Moriwaki H, et al. Inducible expression of lectin-like oxidized LDL receptor-1 in vascular endothelial cells. Circ Res 1998;83:322–37.
[22] Mukai E, Kume N, Hayashida K, et al. Heparin-binding EGF-like growth factor induces expression of lectin-like oxidized LDL receptor-1 in vascular smooth muscle cells. Atherosclerosis 2004;176:289–96.
[23] Aoyama T, Fujiwara H, Masaki T, Sawamura T. Induction of lectin-like oxidized LDL receptor by oxidized LDL and lysophosphatidylcholine in cultured endothelial cells. J Mol Cell Cardiol 1999;31:2101–14.
[24] Kataoka H, Kume N, Miyamoto S, et al. Expression of lectinlike oxidized low-density lipoprotein receptor-1 in human atherosclerotic lesions. Circulation 1999;99:3110–7.
[25] Shin HK, Kim YK, Kim KY, Lee JH, Hong KW. Remnant lipoprotein particles induce apoptosis in endothelial cells by NAD(P)H oxidase-mediated production of superoxide and cytokines via lectin-like oxidized low-density lipoprotein receptor-1 activation: prevention by cilostazol. Circulation 2004;109:1022–8.

Please cite this article in press as: Aramaki Y, et al., Lectin-like oxidized LDL receptor-1 (LOX-1) acts as a receptor for remnant-like lipoprotein particles (RLPs) and mediates RLP-induced migration of vascular smooth muscle cells, Atherosclerosis (2008), doi:10.1016/j.atherosclerosis.2007.12.017

[26] Park SY, Lee JH, Kim YK, et al. Cilostazol prevents remnant lipoprotein particle-induced monocyte adhesion to endothelial cells by suppression of adhesion molecules and monocyte chemoattractant protein-1 expression via lectin-like receptor for oxidized low-density lipoprotein receptor activation. J Pharmacol Exp Ther 2005;312:1241–8.

[27] Jawien A, Bowen-Pope DF, Lindner V, Schwartz SM, Clowes AW. Platelet-derived growth factor promotes smooth muscle migration and intimal thickening in a rat model of balloon angioplasty. J Clin Invest 1992;89:507–11.

[28] Redmond EM, Cahill PA, Hirsch M, et al. Effect of pulse pressure on vascular smooth muscle cell migration: the role of urokinase and matrix metalloproteinase. Thromb Haemost 1999;81:293–300.

[29] Chen M, Narumiya S, Masaki T, Sawamura T. Conserved C-terminal residues within the lectin-like domain of LOX-1 are essential for oxidized low-density-lipoprotein binding. Biochem J 2001;355:289–96.

[30] Higashiyama S, Nanba D. ADAM-mediated ectodomain shedding of HB-EGF in receptor cross-talk. Biochim Biophys Acta 2005; 1751:110–7.

Please cite this article in press as: Aramaki Y, et al., Lectin-like oxidized LDL receptor-1 (LOX-1) acts as a receptor for remnant-like lipoprotein particles (RLPs) and mediates RLP-induced migration of vascular smooth muscle cells, Atherosclerosis (2008), doi:10.1016/j.atherosclerosis.2007.12.017

Circ J 2008; **72:** 420–426

Action of Aspirin on Whole Blood-Aggregation Evaluated by the Screen Filtration Pressure Method

Arata Tabuchi, MD; Ryoji Taniguchi, MD*; Kanako Takahashi, MT*; Hirokazu Kondo, MD*; Mitsunori Kawato, MD*; Takeshi Morimoto, MD, MPH**; Takeshi Kimura, MD*; Toru Kita, MD*; Hisanori Horiuchi, MD*

Background There are few monitoring systems widely used in clinical practice for evaluating the effectiveness of aspirin therapy, so in the present study aspirin's antiplatelet effects we investigated with a whole blood aggregometer using a screen filtration pressure (SFP) method.

Methods and Results Thirty-five healthy male volunteers took 100 mg/day aspirin for 14 days. Whole-blood aggregation was analyzed at baseline and on days 7 and 14, using collagen and adenosine diphosphate as the stimuli, and compared with the platelet-rich plasma (PRP) aggregation measured by optical aggregometer. The platelet-aggregation threshold index (PATI) for both methods, which was defined as the putative agonist-concentration giving half-maximal aggregation, and the PRP-maximal aggregation rate were analyzed. The maximal aggregation rate induced by 1.6 mg/L collagen decreased from 85.5% (80.8–92.8) [median (interquartile range)] at baseline to 51.5% (39–63.8) on day 14 ($p<0.0001$). The PRP-PATI and whole-blood PATI for collagen increased from 0.32 (0.28–0.70) to 1.82 mg/L (1.25–2.89) ($p<0.0001$) and from 0.28 (0.22–0.3) to 1.06 mg/L (1.01–1.29) ($p<0.0001$) respectively.

Conclusions The whole-blood PATI and PRP-PATI for collagen, as well as the maximal PRP aggregation rate, clearly distinguish platelet aggregability before and after aspirin intake. However, whole-blood analysis by the SFP-method is easier to perform, and is a promising method of monitoring aspirin's effects. (*Circ J* 2008; **72:** 420–426)

Key Words: Aggregation; Aspirin; Platelet-aggregation threshold index (PATI); Screen filtration pressure method; Whole blood-aggregation

Aspirin is an irreversible inhibitor of cyclooxygenase-1, which is the rate-limiting enzyme for producing thromboxane A_2 in platelets.[1] Aspirin is the antiplatelet drug used most widely and its effect on prevention of cardiovascular events has been established for high-risk patients.[2–4] However, the efficacy of aspirin is rarely monitored in clinical practice because valid and comprehensive monitoring systems have not yet been established.

Platelet aggregation has conventionally been examined by the optical aggregometer method, in which a change in the light transmission of platelet-rich plasma (PRP) is monitored under agonist stimulation at certain concentrations.[5] Requirement of centrifugation for the preparation of PRP is one of the hindrances to its routine use. In addition, the PRP method measures the aggregability of platelets alone, whereas in vivo other blood cells also regulate thrombus formation by modulating platelet aggregation; for example, leukocytes produce platelet activating factor[6] and erythrocytes bind prostacyclin to inhibit its activity.[7] Therefore, if whole-blood aggregation is properly measured, it might reflect a more physiological phenomenon. Several systems for measuring whole-blood aggregation, such as the PFA-100® (Dade-Behring, Deerfield, IL, USA), Verify-Now® (Accumetrics, San Diego, CA, USA) and ROTEM analyzer® (Pentapharm, Munich, Germany), have been developed and are under investigation for establishment as a clinical test.

The screen filtration pressure (SFP) method was established in the 1960s to analyze whole-blood aggregation by measuring the absorbing pressure of agonist-stimulated whole blood through a microsieve.[8,9] Although the principle of this method is simple and understandable, it has not been widely used, until recently, when a semi-automatic aggregometer that uses this method was developed and has come into use in the clinical and research fields.[10–12] Using this aggregometer, we have been able to measure whole-blood aggregability quickly and reproducibly.

In the current study, 35 healthy male volunteers took aspirin for 14–21 days and the whole-blood and PRP aggregations were monitored by whole-blood aggregometer and optical aggregometer, respectively.

Methods

Study Population and Procedures

This study was approved by the Ethics Committee, Faculty of Medicine, Kyoto University. Thirty-five healthy male physicians aged 26–48 years (35±5.5 years old) voluntarily participated after giving informed consent. Each subject took 100 mg enteric-absorbed aspirin® (Bayer, Leverkusen, Germany) after breakfast for 14 days. Fasting

(Received July 6, 2007; revised manuscript received October 12, 2007; accepted November 13, 2007)

*Departments of Geriatric Medicine, *Cardiovascular Medicine and **Medical Education, Graduate School of Medicine, Kyoto University, Kyoto, Japan*

Mailing address: Hisanori Horiuchi, MD, Department of Cardiovascular Medicine, Graduate School of Medicine, Kyoto University, Kyoto 606-8507, Japan. E-mail: horiuchi@kuhp.kyoto-u.ac.jp

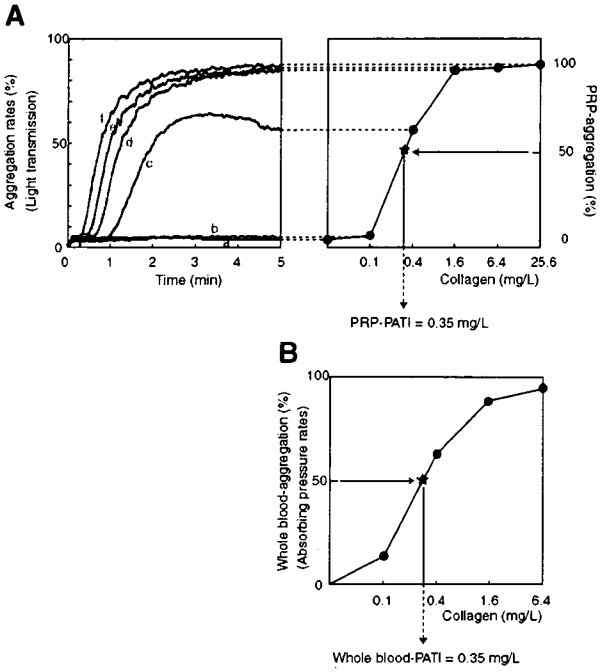

Fig 1. Definition of platelet-aggregation threshold index (PATI). Definitions and methods of calculation of platelet-rich plasma (PRP) (A) and whole-blood (B) PATI are shown schematically. (A, Left) Light transmission curves obtained with 0 (a), 0.1 (b), 0.4 (c), 1.6 (d), 6.4 (e) and 25.6 mg/L (f) of collagen. (B) 0% and 100% absorbing pressure rates represent −6 mmHg and −130 mmHg, respectively.

blood samples were collected in the morning before aspirin intake. Measurements were made at baseline and on days 7 and 14. Nine of the subjects took 300 mg/day aspirin for 7 days following the 14-day period of 100 mg/day aspirin intake and their fasting blood samples were analyzed on day 21.

Measurement of PRP- and Whole-Blood Aggregation

After placement of a tourniquet, blood was collected from an arm vein using a 21G needle and placed in a glass tube containing a final concentration of 0.313% sodium citrate. The effect of the tourniquet on both forms of aggregation was negligible when blood collection was performed smoothly (data not shown), as described before![10] PRP was prepared by centrifugation of blood at 200 G at 25°C for 10 min and platelet-poor plasma was prepared by centrifugation at 2,000 G at 25°C for 10 min. Aggregability immediately after blood collection was weaker, but stabilized at a later time![10,13] Because the aggregability of the PRP and whole blood was stable during the 60–120 min after blood collection (data not shown), we analyzed aggregability during that period.

Horse tendon collagen (Horm®) was purchased from Nycomed (Munich, Germany) and adenosine diphosphate (ADP) from Sigma (St Louis, MO, USA). PRP aggregation was measured by the addition of 20 μl of collagen (final concentrations: 0, 0.1, 0.4, 1.6, 6.4, and 25.6 mg/L) and ADP (0, 1, 3, 9, 27, and 100 μmol/L) to 180 μl of PRP while constantly stirring at 37°C using a light transmission aggregometer, MCM HEMA TRACER 212® (MC Medical, Tokyo, Japan). The degree of light transmission of the PRP was defined as showing an aggregation rate of 0% and that of the platelet-poor plasma as 100%. The platelet-aggregation threshold index (PATI) was defined as the putative agonist-concentration giving 50% aggregation based on the light transmission rate at 5 min after stimulation (Fig 1A). The light transmission rate at 5 min during stimulation by an excessively high concentration of 25.6 mg/L of collagen or 100 μmol/L of ADP was defined as 100% of PRP aggregation and the rate without agonist stimulation as 0%. In most cases, the aggregation rates at 5 min obtained with 25.6 mg/L of collagen and 100 μmol/L of ADP were similar to those obtained with 6.4 mg/L of collagen and 27 μmol/L of ADP, respectively (data not shown), indicating that PRP aggregation was saturated at 6.4 mg/L of collagen and 27 μmol/L of ADP.

Whole-blood aggregation was measured with a whole-blood aggregometer using the SFP method (WBA-Neo®; ISK, Tokyo, Japan). The reaction was started by the addition of 20 μl of agonist solution to 180 μl of whole blood while constantly stirring at 37°C. The final concentrations of collagen were 0.1, 0.4, 1.6, and 6.4 mg/L, and those of ADP were 1, 3, 9, and 27 μmol/L. At 5 min after stimulation, the absorbing pressure of aggregated whole blood was measured through a microsieve with 30×30 μm windows, and a negative pressure of −130 mmHg was defined as 100% of aggregation and −6 mmHg as 0%, the latter deviation from 0 mmHg being designated because of the viscosity of unstimulated whole blood![10] As shown in Fig 1B, the putative agonist-concentration giving 50% aggregation was calculated and defined as the PATI![10]

Whole-blood aggregation was measured in triplicate and PRP-aggregation in duplicate, and the average value of these measurements was analyzed.

Laboratory Testing

General serum values were measured by the SRL Laboratory (Tokyo, Japan).

Table 1 Clinical and Biochemical Characteristics

	Baseline	*Day 7*	*Day 14*
Age, years	35±5.5		
Body mass index, kg/m²	23.7±2.5	*NT*	*NT*
RBC, ×10¹²/L	4.98±0.35	4.94±0.36	4.93±0.37
Hemoglobin, ×10²g/L	1.54±0.87	1.53±0.11	1.52±0.11
WBC, ×10⁹/L	5.90±1.00	5.89±1.07	5.86±1.27
Platelets, ×10¹¹/L	2.32±0.48	2.35±0.39	2.41±0.43
Fibrinogen, g/L	2.29±0.47	*NT*	*NT*
PT (INR)	1.05±0.07	*NT*	0.95±0.30*
aPTT, s	35.8±5.0	*NT*	33.2±11.5
Fasting glucose, g/L	1.00±0.11	*NT*	*NT*
AST, IU/L	23±8	*NT*	*NT*
ALT, IU/L	30±25	*NT*	*NT*
Total cholesterol, g/L	2.01±0.26	*NT*	1.98±0.29
HDL-cholesterol, g/L ♂	0.58±0.13	*NT*	0.57±0.15
LDL-cholesterol, g/L	1.19±0.21	*NT*	1.06±0.42
Triglyceride, g/L	1.19±0.53	*NT*	1.26±0.92
BUN, mg/L	13.4±2.8	*NT*	*NT*
Creatinine, mg/L	8.7±0.9	*NT*	*NT*
Na, mmol/L	141±1.9	*NT*	*NT*
K, mmol/L	4.5±0.6	*NT*	*NT*
hs-CRP μg/L	719±1,420	721±1,690	700±1,330

*Data are means±SD; males=35. *p<0.05 compared with baseline by Wilcoxon's ranked test.*

NT, not tested; RBC, erythrocyte; WBC, leukocyte; PT (INR), prothrombin time (international normalized ratio); aPTT, activated partial thromboplastin time; AST, aspartate transaminase; ALT, alanine transaminase; HDL, high-density lipoprotein; LDL, low-density lipoprotein; BUN, blood urea nitrogen; hs-CRP, high-sensitivity C-reactive protein.

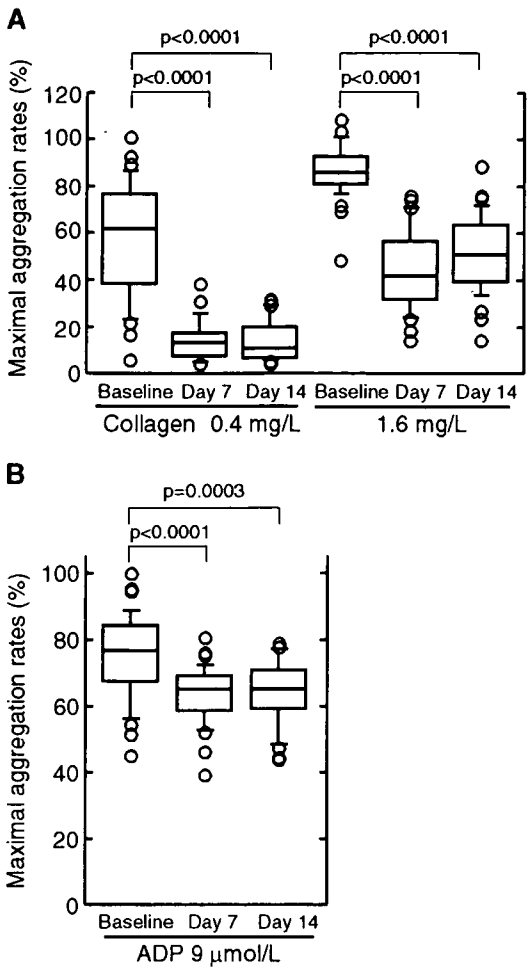

Fig 2. Effects of aspirin intake on maximal aggregation rates of platelet-rich plasma. Maximal aggregation rates induced with 0.4 and 1.6 mg/L of collagen (A) and 9 μmol/L of adenosine diphosphate (ADP) (B) were measured at baseline, and on days 7 and 14 of 100 mg/day aspirin intake as described in the text (n=35). The box–whisker plots show the median, 25th and 75th percentiles (boxes), and the 10th and 90th percentiles (whiskers).

Statistical Analysis

Statistical analysis was performed using Excel® (Microsoft, Redmond, WA, USA) and Statview® (SAS Institute, Cary, NC, USA). Aggregation rates and PATI values are presented as median (interquartile range) and other data as means ± SD. Wilcoxon's signed-rank test was used for statistical analysis. Correlations between valuables were analyzed using Spearman's correlation; $p<0.05$ was considered significant. Receiver operator-characteristics (ROC) analysis for the detection of aspirin intake was performed using the values obtained from both PRP- and whole-blood aggregation measurements. In some figures, data are shown using box and whisker plots in which the boxes show median and interquartile ranges, and bars represent the 10th and 90th percentiles, with the median representing the 18th value among 35 subjects. The lower boundary of the box represents the 10th value and the upper one shows the 26th value. The lower bar represents the 4th value and the upper bar shows the 32nd value. Upper and lower open circles represent the 1st to 3rd and the 33rd to 35th values respectively.

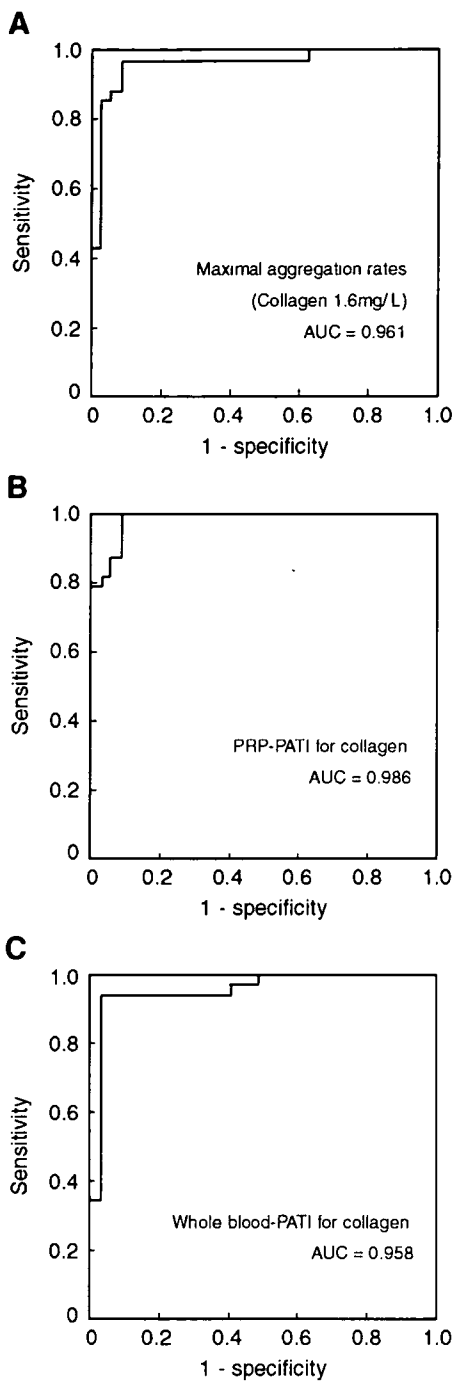

Fig 3. Receiver-operator-characteristics (ROC) curve analysis. ROC curves of maximal aggregation rates with 1.6 mg/L of collagen stimulation (A), PRP-PATI for collagen (B) and whole-blood PATI for collagen (C) in detecting the intake of aspirin. AUC, area under the curve. See Fig 1 for other abbreviations.

Results

Baseline Characteristics

None of the 35 volunteers took drugs that would affect platelet aggregation for 7 days before the study began or at any time during the study. Laboratory tests for the group as a whole were normal (Table 1), and none of the individual subjects had values that lay outside the normal range. None

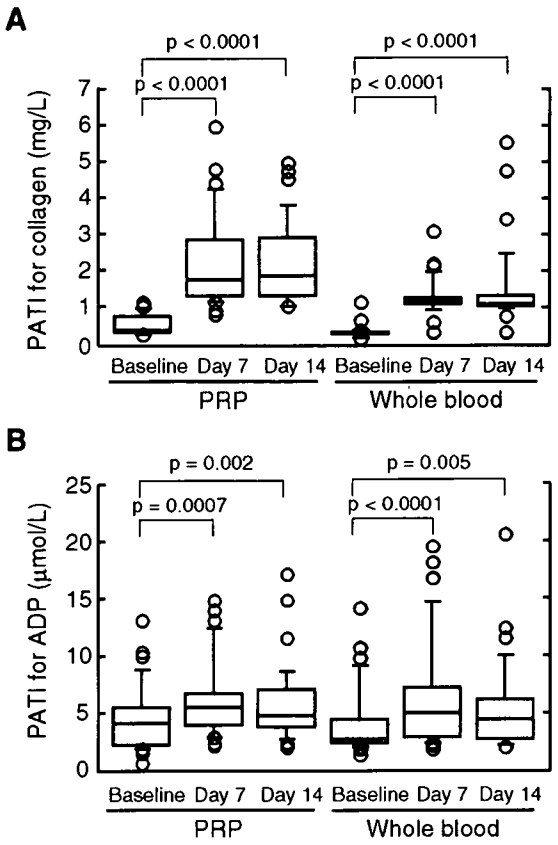

Fig 4. Effects of aspirin intake on the PRP-PATI and whole-blood PATI for collagen (A) and ADP (B). All values were analyzed at baseline and on days 7 and day of 100 mg/day aspirin intake as described in the text (n=35). The box-whisker plots show the median, the 25th and 75th percentiles (boxes), and the 10th and 90th percentiles (whiskers). See Figs 1 and 2 for abbreviations.

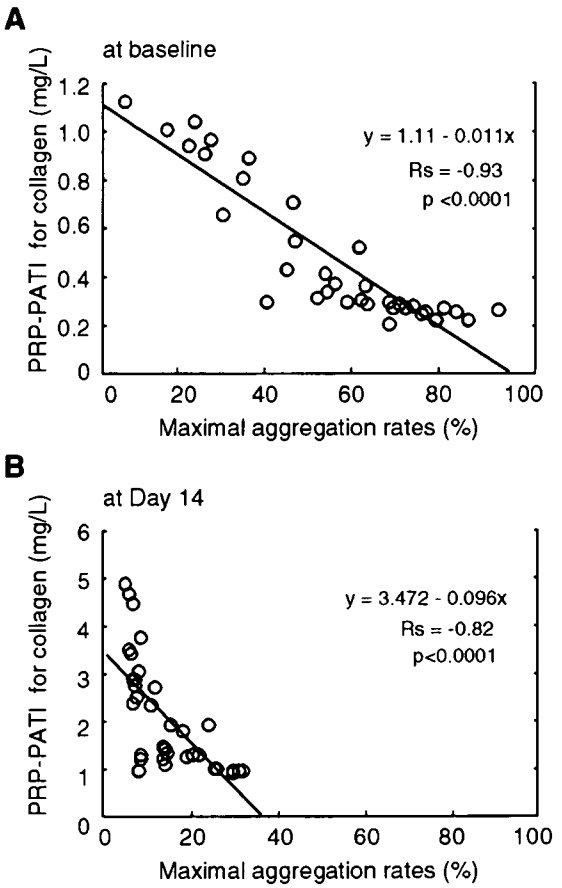

Fig 5. Correlation of the PRP-PATI for collagen and the maximal aggregation rate induced with 0.4 mg/L of collagen. The PRP-PATI and the maximal aggregation rate at baseline (A) and on day 14 (B) for individuals are plotted. Rs, Spearman rank correlation coefficient. See Fig 1 for abbreviations.

of the factors shown in Table 1, including platelet and other blood-cell counts, correlated with either collagen- or ADP-induced PRP- aggregability or whole-blood aggregability at baseline or on day 14 (data not shown). None of the laboratory tests subjected to serial testing showed a significant change before and after aspirin intake, except prothrombin time (PT), but the PT values at both baseline and on day 14 were within the normal range (Table 1).

Effect of Aspirin on the Maximal Rate of PRP Aggregation

The maximal aggregation rates for collagen were decreased by aspirin in all 35 subjects. The rates induced by 0.4 mg/L of collagen were 62.0% (38.3–76.6) [median (interquartile range)] at baseline, 13.0% (7.6–17.5) on day 7 and 11.0% (6.5–19.6) on day 14 (Fig 2A), the latter 2 values significantly different from baseline ($p<0.0001$). The rates induced by 1.6 mg/L collagen also decreased significantly from 85.5% (80.8–92.8) at baseline to 41.5% (31.9–56.4) on day 7 ($p<0.0001$) and 50.5% (39.0–63.8) on day 14 ($p<0.0001$) (Fig 2A). The rates induced by 1.6 mg/L of collagen were distributed evenly and the rates in 29 subjects (10–90th percentile) were in the range of 76.5–108.5% at baseline and 33–69.5% on day 14 (Fig 2A). The area under the ROC curves analyzing the rates at baseline and on day 14 for those induced by collagen at 0.4 mg/L (data not shown) and 1.6 mg/L (Fig 3A) was 0.947 and 0.961, respectively. The maximal aggregation rates with 0.4–1.6 mg/L of collagen appeared useful for evaluating aspirin's effect on inhibition of platelet aggregation, although the ranges of these rates was distributed rather widely (Fig 2A).

We also analyzed the maximal aggregation rate induced by ADP. As shown in Fig 2B, aspirin significantly decreased the rate induced by 9 μmol/L of ADP from 76.5% (67.3–84.3) at baseline to 65.0% (58.1–69.0) on day 7 ($p<0.0001$) and to 65.0% (58.9–70.8) on day 14 ($p=0.0003$) (Fig 2B). However, the decreases were small and the rates were widely distributed and extensively overlapped.

Effect of Aspirin on PRP-PATI for Collagen and ADP

The PRP-PATI for collagen was increased by aspirin in all 35 subjects: 0.32 mg/L (0.28–0.70) at baseline, 1.74 mg/L (1.27–2.84) on day 7, and 1.82 mg/L (1.25–2.89) on day 14 (Fig 4A). Aspirin intake significantly increased the PRP-PATI for collagen on both day 7 ($p<0.0001$) and day 14 ($p<0.0001$), compared with baseline. PRP-PATI values for collagen were distributed evenly and the values in 29 subjects (10–90th percentile) were in the range of 0.23–0.97 mg/L at baseline and 1.00–3.80 mg/L on day 14 (Fig 4A). The PRP-PATI for collagen negatively well-correlated with the maximal aggregation rate induced by 0.4 mg/L collagen at base-

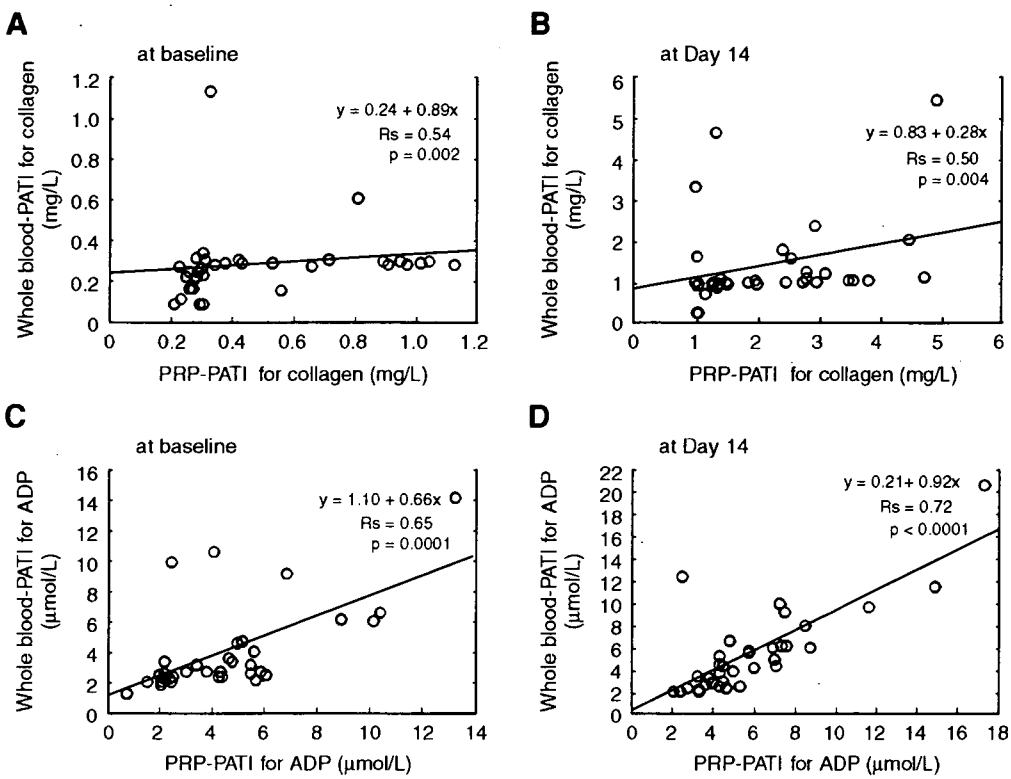

Fig 6. Correlation between the whole-blood and PRP-PATI values. Collagen stimulation at baseline (A) and on day 14 (B). ADP stimulation at baseline (C) and on day 14 (D). See Figs 1 and 2 for abbreviations.

line (Rs=–0.93; p<0.0001) (Fig 5A) and on day 14 (Rs= –0.82; p<0.0001) (Fig 5B). Similar negative correlations were observed with 1.6 mg/L collagen at both baseline (Rs= –0.39; p=0.02) and on day 14 (Rs=–0.72; p<0.0001) (data not shown). The area under the ROC curve analyzing the PRP-PATI for collagen at baseline and on day 14 was 0.986 (Fig 3B). Thus, the PRP-PATI for collagen clearly distinguished aggregability under aspirin intake from that at baseline.

As shown in Fig 4B, aspirin-intake significantly increased the PRP-PATI for ADP from 4.21 μmol/L (2.20–5.53) at baseline to 5.64 μmol/L (3.95–6.79) on day 7 (p=0.0007) and 4.78 μmol/L (3.80–7.13) on day 14 (p=0.002) (Fig 4B). However, the increases were small, and the PATI values were widely distributed and extensively overlapped (Fig 4B).

Effect of Aspirin on PATI of Whole-Blood Aggregation

Whole-blood aggregation was analyzed by semi-automatic aggregometer using the SFP method and the whole-blood PATI for collagen was increased by aspirin in all 35 subjects: 0.28 mg/L (0.22–0.30) at baseline, 1.10 mg/L (1.05–1.22) on day 7, and 1.06 mg/L (1.01–1.29) on day 14 (Fig 4A). Thus, aspirin intake significantly increased the whole-blood PATI for collagen on both day 7 (p<0.0001) and day 14 (p<0.0001), compared with baseline. The whole-blood PATI for collagen in 29 subjects (10–90th percentile) at baseline was in the range of 0.15–0.31 mg/L and 0.93–2.43 mg/L on day 14 (Fig 4A). Importantly these values were distributed in a quite narrower range, as compared with the maximal aggregation rate and the PRP-PATI (Figs 2A,4A), and clearly demonstrated differences in aggregability before and after aspirin intake. The ROC curve analysis revealed that the area under the curve analyzing the whole-blood PATI for collagen at baseline and on day 14 was 0.958 (Fig 3C).

As shown in Fig 4B, aspirin-intake slightly increased the whole-blood PATI for ADP from 2.75 μmol/L (2.35–4.56) at baseline to 4.97 μmol/L (3.03–7.26) on day 7 (p<0.0001), and to 4.45 μmol/L (2.75–6.26) on day 14 (p=0.005) (Fig 4B). However the distribution was wide with extensive overlapping.

Comparison of Whole-Blood PATI and PRP-PATI

As shown in Figs 6A,B, there was a moderate correlation between the PRP-PATI and whole-blood PATI for collagen at both baseline (Rs=0.54; p=0.002) and on day 14 (Rs= 0.50; p=0.004), whereas the PRP-PATI and whole-blood PATI for ADP were well correlated at both baseline (Rs= 0.65; p=0.0001) (Fig 6C) and on day 14 (Rs=0.72; p<0.0001) (Fig 6D).

Effect of High-Dose Aspirin on Whole-Blood and PRP Aggregations Induced by Collagen

Among the participating 35 subjects, 9 took 300 mg/day aspirin for 7 days following the administration of 100 mg/day of aspirin for 14 days. As shown in Figs 7A,B, the higher dose of aspirin did not increase either the PRP-PATI or whole-blood PATI (p=0.44 and 0.41, respectively). On day 21, the PRP-PATI was 1.96 mg/L (1.36–3.22) and the whole-blood PATI was 1.07 mg/L (1.03–1.08), which did not differ significantly from the values on day 14 [PRP-PATI: 1.82 mg/L (1.35–2.78), whole-blood PATI: 1.05 mg/L (0.99–1.07)]. However, the whole-blood PATI for collagen appeared to be more constant during day 7–21, compared

with the PRP-PATI values for collagen (Figs 7A,B).

Discussion

A semi-automatic whole-blood aggregometer that uses the SFP method has been recently developed, and is considered to be useful in clinical practise. It is a simple and rapid whole-blood assay that requires a small amount of blood (1–2 ml). It has been reported that this whole blood aggregometer can detect the reduction of platelet-aggregability in vitro caused by antiplatelet drugs such as aspirin, cilostazol, dipyridamole and tirofiban.[9] To evaluate the utility of this whole-blood aggregometer in clinical practise, we analyzed whole-blood aggregation by the SFP method during daily aspirin intake for 2–3 weeks, and compared the results with those for PRP aggregation, which is the current standard method. As reported previously, the maximal aggregation rate as determined by PRP aggregation showed an excellent ability to distinguish platelet aggregability before and after aspirin intake. In the present study the PRP-PATI for collagen was well correlated with the maximal aggregation rate, and also clearly distinguished platelet aggregability before and after aspirin intake. We also found that the whole-blood PATI for collagen accurately distinguished platelet aggregability before and after aspirin intake. Moreover, the whole-blood-PATI values were distributed in a much narrower range than the PRP-PATI values. Therefore, together with its feasibility, whole-blood aggregation measured with the SFP method is an excellent index for monitoring the efficacy of aspirin therapy.

At present, the maximal aggregation rate measured by optical aggregometer is the standard index for platelet aggregability. However, in the present study the distribution of the individual maximal aggregation rates appeared rather wide (Figs 2A,B), so to try and improve this measurement, we analyzed the PRP-PATI, defined as the putative agonist-concentration giving half-maximal aggregation. In that case, the values for collagen clearly distinguished platelet aggregability before and after aspirin intake (Fig 4A). Also, the area under the ROC curve obtained with the maximal aggregation rate was 0.961 (Fig 3A) and that using the PRP-PATI was 0.986 (Fig 3B). The PRP-PATI for collagen in 90% of cases was below 0.96 mg/L at baseline and in 90% of cases was over 1 mg/L on day 14. Therefore, a PRP-PATI for collagen of approximately 1 mg/L seems a reasonable cut-off value for distinguishing the effects of aspirin intake. A cut-off value between 0.966 and 0.973 mg/L gave 91% sensitivity and 100% specificity, whereas a value between 69.5% and 76.5% of maximal aggregation rate stimulated with 1.6 mg/L of collagen gave 97% sensitivity and 91% specificity. In general, the PATI is a more comprehensible index that has its own significant meaning, whereas the maximal aggregation rate must be interpreted according to the concentration of agonist. The present results suggest that the PRP-PATI may be preferred for monitoring aspirin's effects.

Analysis of whole-blood aggregation has the obvious advantage of easy and rapid sample preparation without the need for centrifugation. Recent improvements in the whole blood aggregometer using the SFP method enabled us to consistently examine many samples. As noted, the whole blood-PATI is defined as the putative agonist-concentration that induces half-maximal absorbing pressure[9] and in the present study gave values for collagen that clearly showed an increase during administration of aspirin, compared with

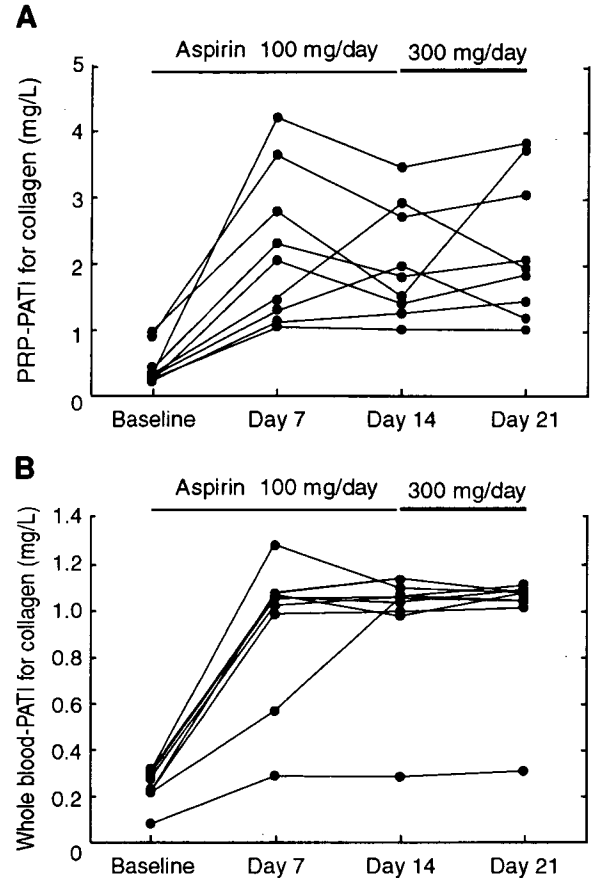

Fig 7. Effects of high-dose aspirin on PRP-PATI (A) and whole-blood PATI (B). Nine subjects took 100 mg/day aspirin for 14 days, followed by 300 mg/day aspirin intake for 7 days. Values were analyzed at baseline and on days 7, 14 and 21. See Fig 1 for abbreviations.

baseline (Fig 4A). Interestingly, the whole-blood PATI values for the 10–90th percentile, especially the 25–75th percentile, were distributed in a narrower range both before and after aspirin intake, and these ranges were also more clearly separated from one another compared with the PRP-PATI values (Fig 4A). The area under the ROC curve obtained with the whole-blood PATI values was 0.958 (Fig 3C). Judging from the distribution (Fig 4A), it seems that approximately 0.7 mg/L is a reasonable cut-off point for the whole-blood PATI for collagen to distinguish the effects of aspirin intake. A cut-off value between 0.61 and 0.74 mg/L gave 94% sensitivity and 97% specificity. These findings suggest that the whole-blood PATI for collagen is an excellent indicator of aspirin's effects as compared with values obtained using the optical aggregometer.

Both the PRP-PATI and whole-blood PATI for ADP also showed significant elevation after aspirin intake, but the increase was relatively small and the distribution of the PATI values was wide and they extensively overlapped before and after aspirin intake (Fig 4B), findings that are consistent with previous investigations.[14,15] Therefore, neither of the PATI values for ADP seem particularly useful for evaluating aspirin's effects.

The PRP-PATI is determined from light transmission rates, whereas the whole-blood PATI is based on the absorbing pressures through a microsieve. Therefore, the 2